Article

CCR5 closes the temporal window for memory linking

https://doi.org/10.1038/s41586-022-04783-1

Received: 24 March 2021

Accepted: 20 April 2022

Published online: 25 May 2022

Check for updates

Yang Shen[1,8], Miou Zhou[1,2,8]✉, Denise Cai[1,3], Daniel Almeida Filho[1], Giselle Fernandes[1], Ying Cai[1], André F. de Sousa[1], Min Tian[4], Nury Kim[5,6], Jinsu Lee[6], Deanna Necula[1], Chengbin Zhou[1], Shuoyi Li[1], Shelbi Salinas[2], Andy Liu[1], Xiaoman Kang[1], Masakazu Kamata[7], Ayal Lavi[1], Shan Huang[1], Tawnie Silva[1], Won Do Heo[6] & Alcino J. Silva[1]✉

Real-world memories are formed in a particular context and are often not acquired or recalled in isolation[1–5]. Time is a key variable in the organization of memories, as events that are experienced close in time are more likely to be meaningfully associated, whereas those that are experienced with a longer interval are not[1–4]. How the brain segregates events that are temporally distinct is unclear. Here we show that a delayed (12–24 h) increase in the expression of C-C chemokine receptor type 5 (CCR5)—an immune receptor that is well known as a co-receptor for HIV infection[6,7]—after the formation of a contextual memory determines the duration of the temporal window for associating or linking that memory with subsequent memories. This delayed expression of CCR5 in mouse dorsal CA1 neurons results in a decrease in neuronal excitability, which in turn negatively regulates neuronal memory allocation, thus reducing the overlap between dorsal CA1 memory ensembles. Lowering this overlap affects the ability of one memory to trigger the recall of the other, and therefore closes the temporal window for memory linking. Our findings also show that an age-related increase in the neuronal expression of CCR5 and its ligand CCL5 leads to impairments in memory linking in aged mice, which could be reversed with a *Ccr5* knockout and a drug approved by the US Food and Drug Administration (FDA) that inhibits this receptor, a result with clinical implications. Altogether, the findings reported here provide insights into the molecular and cellular mechanisms that shape the temporal window for memory linking.

Memory formation can be affected by previous experiences. For example, memories acquired close in time often become linked such that the retrieval of one increases the likelihood of retrieving the other (memory linking). Abnormal memory linking (for example, improper relational memory) is involved in psychiatric disorders such as post-traumatic stress disorder and schizophrenia[8,9]. However, very little is known about the mechanisms that regulate interactions amongst memories. Activation of CREB and subsequent increases in neuronal excitability are thought to open the temporal window for memory linking, so that a given neuronal ensemble involved in encoding one memory is more likely to participate in encoding a second memory acquired close in time[2,10–13]. Accordingly, the neuronal overlap between memory ensembles has been shown to be critical for memory linking[1–3]. By contrast, little is known about the mechanisms that segregate events that are temporally distinct. CCR5 has been extensively studied in the context of inflammatory responses and HIV infection[6,7]. However, comparatively little is known about its role in learning and memory. Both CCR5 and CCL5 are highly enriched in the CA1 region of the hippocampus[14–16], and CCR5 is a negative regulator of CREB activation and neuronal excitability[15,17]. Here we show that a gradual increase in the expression of CCL5 and CCR5 after memory formation closes the temporal window for memory linking, thus segregating memories that are temporally distinct.

CCR5 expression is enhanced after learning

To investigate the role of CCR5 in contextual memory linking, in which the memory of one context is associated with or linked to the memory of a second context[1], we first tested whether the expression of CCR5 and its ligands changes after contextual fear conditioning (Fig. 1a) in a brain region critical for this form of learning (dorsal CA1; dCA1). Compared to expression levels in mice that stayed in their home cage, the levels of both *Ccr5* and *Ccl5* mRNA increased 12 h after contextual conditioning (Fig. 1b, c), whereas there were no significant changes in the expression of other CCR5 ligands tested (*Ccl3*, *Ccl4* and *Ccl11*; Extended Data Fig. 1a–d). Next, we used in situ hybridization to determine the hippocampal cellular distribution of this learning-induced increase in *Ccr5* expression (Fig. 1d). Although in dCA1 of mice that

[1]Neurobiology, Psychiatry and Psychology Departments and Integrative Center for Learning and Memory, University of California Los Angeles, Los Angeles, CA, USA. [2]Graduate College of Biomedical Sciences, Western University of Health Sciences, Pomona, CA, USA. [3]Neuroscience Department, Icahn School of Medicine, New York, NY, USA. [4]Department of Neurology, David Geffen School of Medicine, University of California Los Angeles, Los Angeles, CA, USA. [5]Center for Cognition and Sociality, Institute for Basic Science, Daejeon, Republic of Korea. [6]Department of Biological Sciences, Korea Advanced Institute of Science and Technology, Daejeon, Republic of Korea. [7]Department of Hematology and Oncology, University of California Los Angeles, Los Angeles, CA, USA. [8]These authors contributed equally: Yang Shen, Miou Zhou. ✉e-mail: mzhou@westernu.edu; silvaa@mednet.ucla.edu

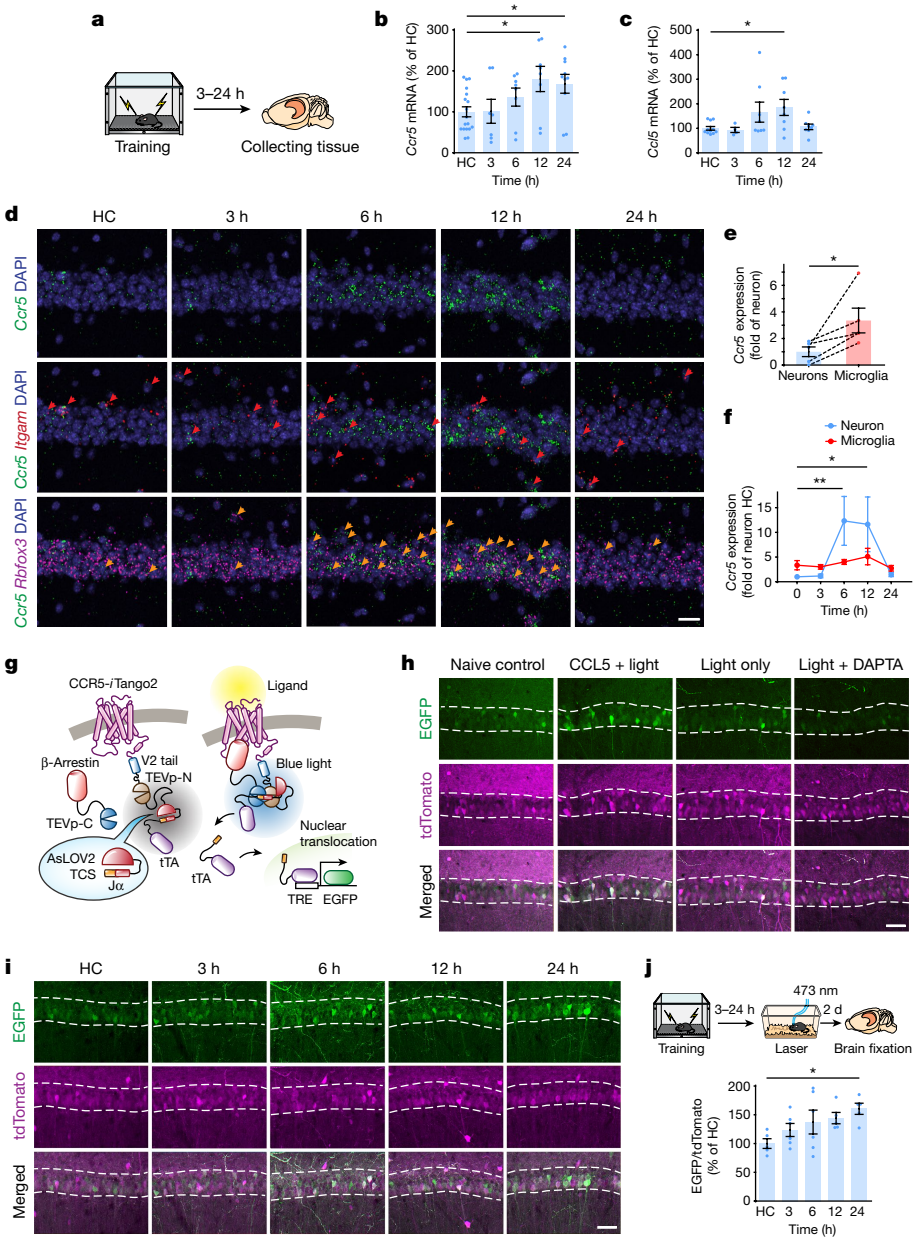

Fig. 1 | CCR5 expression and activation in the dorsal hippocampus after contextual fear conditioning. a–**c**, mRNA levels of *Ccr5* (**b**) and *Ccl5* (**c**) in mouse dCA1 at 3–24 h after fear conditioning (**a**). Tissue (dCA1) from home cage (HC) mice was collected at the same time points (3–24 h) and pooled together as the control HC group. Results were normalized to HC (*Ccr5*: HC $n = 18$, 3 h $n = 7$, 6 h $n = 8$, 12 h $n = 8$, 24 h $n = 10$ mice; *Ccl5*: HC $n = 11$, 3 h $n = 4$, 6 h $n = 8$, 12 h $n = 8$, 24 h $n = 8$ mice; $^*P < 0.05$, one-way ANOVA). **d**, Representative images of the mRNA expression of *Ccr5*, *Itgam* (a microglial marker) and *Rbfox3* (a neuronal marker) in dCA1 from naive mice or mice 3–24 h after fear conditioning. Red arrows: cells expressing *Ccr5* and *Itgam*. Orange arrows: cells expressing *Ccr5* and *Rbfox3*. Scale bar, 20 μm. **e**, Number of *Ccr5*-expressing microglia and neurons in naive mice ($n = 5$ mice per group; $^*P < 0.05$, paired *t*-test). **f**, Number of *Ccr5*-expressing microglia and neurons 3–24 h after fear conditioning (HC $n = 5$, 3 h $n = 4$, 6 h $n = 5$, 12 h $n = 4$, 24 h $n = 4$ mice; $^*P < 0.05$, $^{**}P < 0.01$, two-way repeated measures ANOVA). **g**, Schematics for CCR5-*i*Tango2. **h**, Representative images of CCR5-*i*Tango2-expressing dCA1 neurons after treatment with CCL5, DAPTA (a CCR5 antagonist) and light stimulation. Scale bar, 50 μm. **i**, Representative images of CCR5-*i*Tango2-expressing dCA1 neurons after fear conditioning. Scale bar, 50 μm. **j**, Quantification of EGFP expression (intensity normalized to tdTomato, which is tagged to β-arrestin through P2A, reflecting expression of the *i*Tango system. HC $n = 5$, 3 h $n = 6$, 6 h $n = 6$, 12 h $n = 5$, 24 h $n = 5$ mice; $^*P < 0.05$, one-way ANOVA). All results are shown as mean ± s.e.m.

stayed in their home cage there were more *Ccr5*-expressing microglia than *Ccr5*-expressing neurons (Fig. 1e), there was a marked increase in *Ccr5*-expressing neurons—but not microglia—at 6 h and 12 h after contextual conditioning (Fig. 1f). Further analysis showed that the increase was mainly in excitatory neurons (Extended Data Fig. 1e, f). Unlike *Ccr5*, in dCA1 of home cage mice there were more *Ccl5*-expressing neurons than *Ccl5*-expressing microglia, which is consistent with a previous report[14], whereas no obvious changes in the number of *Ccl5*-expressing neurons or microglia were observed (Extended Data Fig. 1g–i). To examine whether *Ccr5* is primarily expressed in memory ensemble cells after learning, we used either the cFos-tTA transgenic mice and AAV-TRE-mCherry virus to label neurons involved in contextual memory, or the optogenetic ($ChR2_{ETTC}$) system (in which neurons express ChR2(E123T/T159C)) to pre-activate a set of neurons before contextual learning to increase the probability that these neurons would be involved in the contextual memory[18]. With both methods, we

found that *Ccr5* had a significantly higher probability of being expressed in memory ensemble cells than chance (Extended Data Fig. 2).

In addition to CCR5 expression, we also measured neuronal CCR5 activity after learning with the *i*Tango2 system[19] (Fig. 1g). The light- and ligand-gated gene expression system that we constructed (CCR5-*i*Tango2) enables cellular expression of a reporter gene (EGFP) only in the presence of both CCR5 ligand(s) and blue-light exposure (detailed information in Methods). When tested in HEK293 cells (Extended Data Fig. 3a–j), in dCA1 (Fig. 1h, Extended Data Fig. 4a–f) or in the dentate gyrus (Extended Data Fig. 3k–m), CCR5-*i*Tango2 showed a notable increase in EGFP expression only when both light and ligand (CCL5) were present, verifying that CCR5-*i*Tango2 is capable of monitoring ligand-dependent activation of CCR5. Therefore, CCR5-*i*Tango2 viruses were injected into mouse dCA1, and three weeks later mice were trained with contextual fear conditioning. Compared to home cage controls, there was a gradual increase in neuronal CCR5 activity in trained mice over time after conditioning (Fig. 1i, j), a result consistent with the delayed expression patterns of CCR5 and CCL5 presented above (Fig. 1b, c, f). Notably, CCR5 activation measured by CCR5-*i*Tango2 also showed a selectivity for memory ensemble cells after learning (Extended Data Fig. 4g–i).

Overall, our results show that after contextual learning there is a delayed (12–24 h) increase in CCL5–CCR5 signalling in dCA1 neurons, especially in the neurons involved in contextual learning.

CCR5 regulates contextual memory linking

To determine whether CCR5 modulates the temporal window for contextual memory linking[1], we first exposed the mice to one context (context A) and five hours, one, two or seven days later we exposed the mice to a second context (context B) (Fig. 2a). Two days later, the mice were given an immediate shock in context B, and then contextual memory linking was tested two days later in context A. During the memory linking test, the five-hour group showed higher freezing (that is, higher linking) than the one-day, two-day or seven-day groups. This result shows that contextual memory linking decreases significantly between five hours and one day, indicating a time course parallel to the increase in CCR5 signalling after learning (Fig. 1). Therefore, we subsequently investigated whether increasing or inhibiting CCR5 signalling affected the temporal window for contextual memory linking.

We first enhanced CCR5 activity by infusing CCL5 into dCA1 four hours after mice were exposed to context A, a time point that preceded the expected endogenous increase in CCR5 signalling. During the contextual memory linking test, compared to the control group, the CCL5 group showed significantly lower freezing in context A, which the mice had explored five hours before context B (Fig. 2b), indicating that increasing CCR5 activity led to an attenuation of contextual memory linking. Notably, mice in both the control and the CCL5 groups had higher freezing in the five-hour context than in a novel context, suggesting that besides the CCL5–CCR5 signalling pathway, other mechanisms—including those involving other CREB inhibitors or inhibitory microcircuits[2]—might also regulate the temporal widow for memory linking. We then tested whether contextual memory linking could be regulated specifically by direct manipulation of neuronal CCR5 activity with a genetically encoded optical tool (Opto-CCR5) with high spatiotemporal precision[20] (Fig. 2c; detailed information in Methods). Consistent with CCR5 activation[21–24], light stimulation of Opto-CCR5 caused a significant enhancement of intracellular Ca^{2+} and a notable increase in phosphorylation of ERK1 and ERK2 (Extended Data Fig. 5a–e, Supplementary Fig. 1). To ensure specific neuronal expression, AAV1-hSyn-Cre was co-injected with Lenti-EF1a-DIO-Opto-CCR5 (or EGFP control virus) into dCA1 (Fig. 2d, Extended Data Fig. 5f). During the contextual memory linking test, only the control group, and not the Opto-CCR5 group, showed evidence of memory linking (higher freezing in context A, which the mice experienced five hours

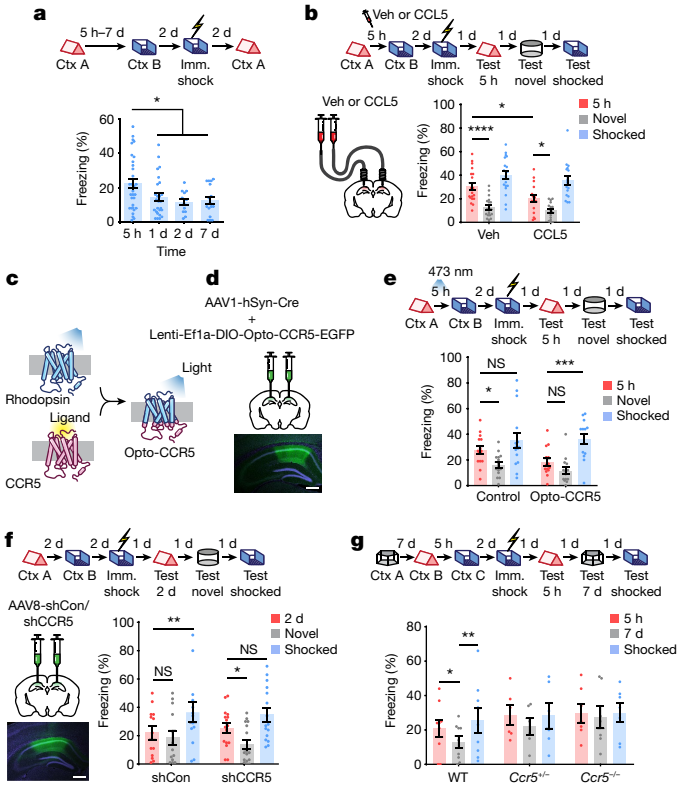

Fig. 2 | CCR5 regulates the temporal window of memory linking. a, Characterization of the temporal window for contextual memory linking (Ctx A, context A; Ctx B, context B; imm. shock, immediate shock; 5 h $n = 32$, 1 d $n = 26$, 2 d $n = 14$, 7 d $n = 16$ mice; $^{*}P < 0.05$, one-way ANOVA). **b**, CCL5 infusion in dCA1 attenuated 5-h contextual memory linking (vehicle (veh) $n = 20$, CCL5 $n = 17$ mice; $^{*}P < 0.05$, $^{****}P < 0.0001$, two-way repeated measures ANOVA). **c**, Schematics of the Opto-CCR5 construct. **d**, Schematics of the injection of viral constructs. Scale bar, 500 µm. **e**, Optogenetic activation of neuronal CCR5 impaired 5-h contextual memory linking (Control $n = 15$, Opto-CCR5 $n = 14$ mice; $^{*}P < 0.05$, $^{***}P < 0.001$, two-way repeated measures ANOVA; NS, not significant). **f**, Left, schematics of AAV8-shCon or AAV8-shCCR5 intrahippocampal injection. Scale bar, 500 µm. Right, knockdown of *Ccr5* in dCA1 neurons extended the temporal window of contextual memory linking (control shRNA (shCon) $n = 13$, shRNA against *Ccr5* (shCCR5) $n = 16$ mice; $^{*}P < 0.05$, $^{**}P < 0.01$, two-way repeated measures ANOVA). **g**, Knockout of *Ccr5* extended the temporal window of contextual memory linking (wild type (WT) $n = 9$, $Ccr5^{+/-}$ $n = 6$, $Ccr5^{-/-}$ $n = 7$ mice; $^{*}P < 0.05$, $^{**}P < 0.01$, two-way repeated measures ANOVA). All results are shown as mean ± s.e.m.

before context B, compared to a novel context; Fig. 2e), confirming that increasing neuronal CCR5 activity specifically after exposure to context A is sufficient to impair contextual memory linking without impairing memory for context B.

To examine whether attenuating CCR5 signalling could extend the window for contextual memory linking, AAV8 containing control short hairpin RNA (shRNA) or shRNA against *Ccr5* was injected into dCA1 (Fig. 2f). Three weeks later, mice were pre-exposed to context A and then context B with a two-day interval. As expected, during testing, the control group did not show memory linking (that is, showed similar freezing in context A to in a novel context; Fig. 2f). By contrast, the *Ccr5* shRNA group showed higher freezing in context A than in a novel context, and there was no difference in freezing between contexts A and B, demonstrating strong memory linking (Fig. 2f).

In addition, *Ccr5* knockout mice ($Ccr5^{-/-}$ mice) were also tested for contextual memory linking. As expected, during the test in context A, the wild-type mice froze less when the interval between contexts was seven days versus five hours. By contrast, $Ccr5^{-/-}$ mice showed

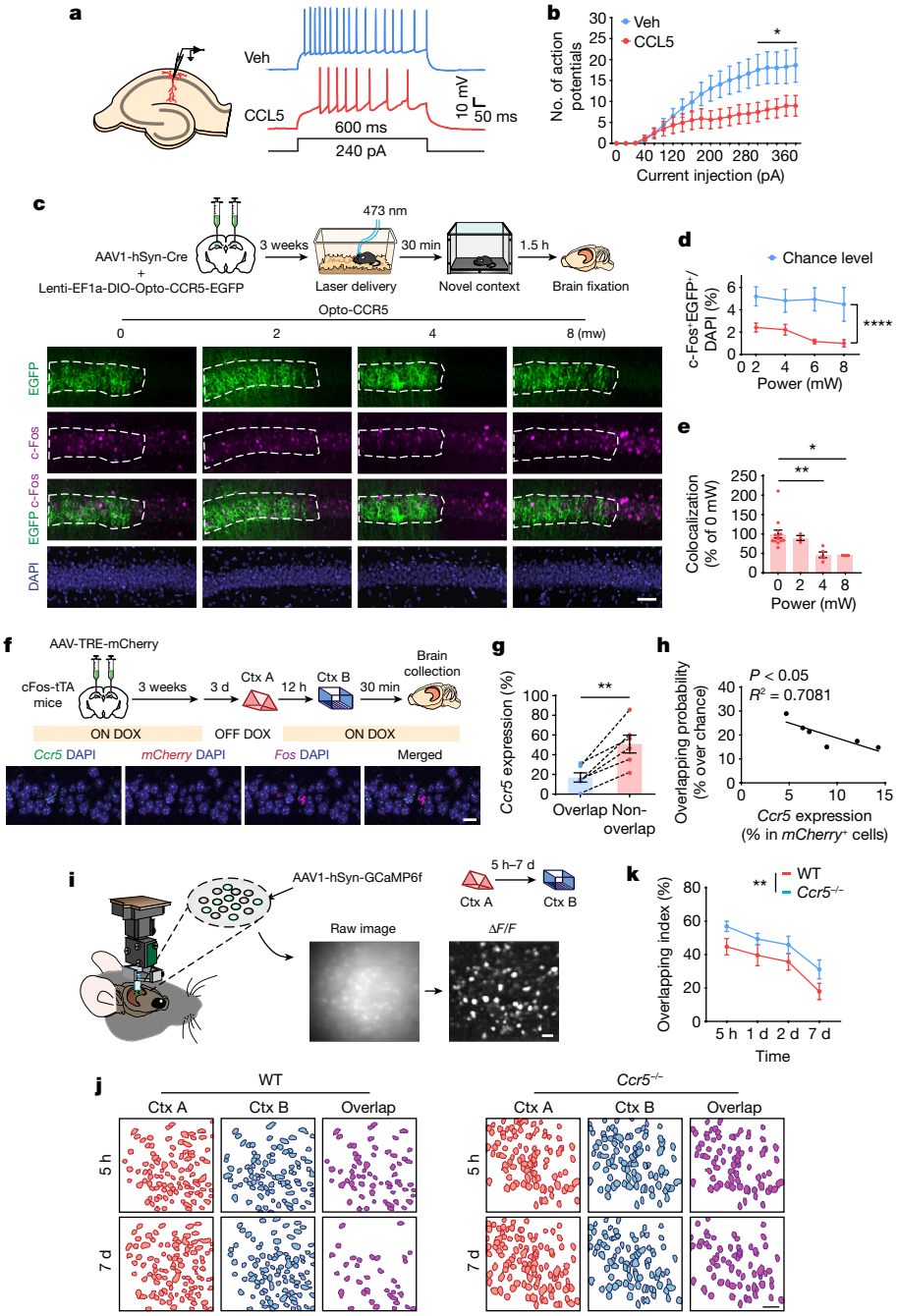

Fig. 3 | CCR5 and CCL5 modulate neuronal excitability, memory allocation and the overlap of memory ensembles. a, Schematics of neuronal recordings and representative traces. **b**, dCA1 neurons treated with CCL5 for 1 h showed a significant decrease in firing rate (Veh control $n = 10$ cells, CCL5 $n = 9$ cells; $^{*}P < 0.05$, two-way repeated measures ANOVA). **c**, Schematics and representative images of colocalization between c-Fos and Opto-CCR5-EGFP after light stimulation and novel context exposure. Scale bar, 50 µm. **d**, Percentage of c-Fos^{+}EGFP^{+} cells at different power levels (0 mW $n = 13$, 2 mW $n = 3$, 4 mW $n = 5$, 8 mW $n = 3$ mice; $^{****}P < 0.0001$, two-way repeated measures ANOVA). **e**, Colocalization between c-Fos^{+} cells and EGFP^{+} cells after normalization to chance level (0 mW $n = 13$, 2 mW $n = 3$, 4 mW $n = 5$, 8 mW $n = 3$ mice; $^{*}P < 0.05$, $^{**}P < 0.01$, one-way ANOVA). **f**, Schematics and representative images of *Ccr5* expression and the overlap between memory ensembles of context A (*mCherry*) and context B (*Fos*) with a 12-h interval between the two contextual exposures. Scale bar, 20 µm. **g**, The probability of *Ccr5* expression in the overlapping cells is lower than that in the non-overlapping cells ($n = 6$ mice; $^{**}P < 0.01$, paired *t*-test). **h**, The probability of ensemble overlap (between context A and context B) and *Ccr5* expression in *mCherry*$^{+}$ cells (ensemble for context A) are negatively correlated ($n = 6$ mice; $R^2 = 0.7081$, $P < 0.05$). **i**, Schematics for miniscope set-up and calcium signal identification. Images were collected from mice exploring different contexts separated by 5 h, 1 d, 2 d or 7 d. Scale bar, 50 µm. **j**, Neuronal overlap between different contexts. Scale bar, 50 µm. **k**, Overlapping index for WT and *Ccr5*$^{-/-}$ mice (WT 5 h–7 d $n = 7$ mice; *Ccr5*$^{-/-}$ 5 h $n = 7$, 1 d–7 d $n = 6$ mice; $^{**}P < 0.01$, two-way ANOVA). All results are shown as mean ± s.e.m.

similar freezing in context A when the interval between context A and B was five hours or seven days. These freezing levels were also similar to those shown in the shocked context (context C; Fig. 2g), showing strong memory linking in *Ccr5*$^{-/-}$ mice with a time interval (that is, seven days), whereas wild-type mice do not show memory linking. Thus, two very different manipulations that decreased the levels of CCR5

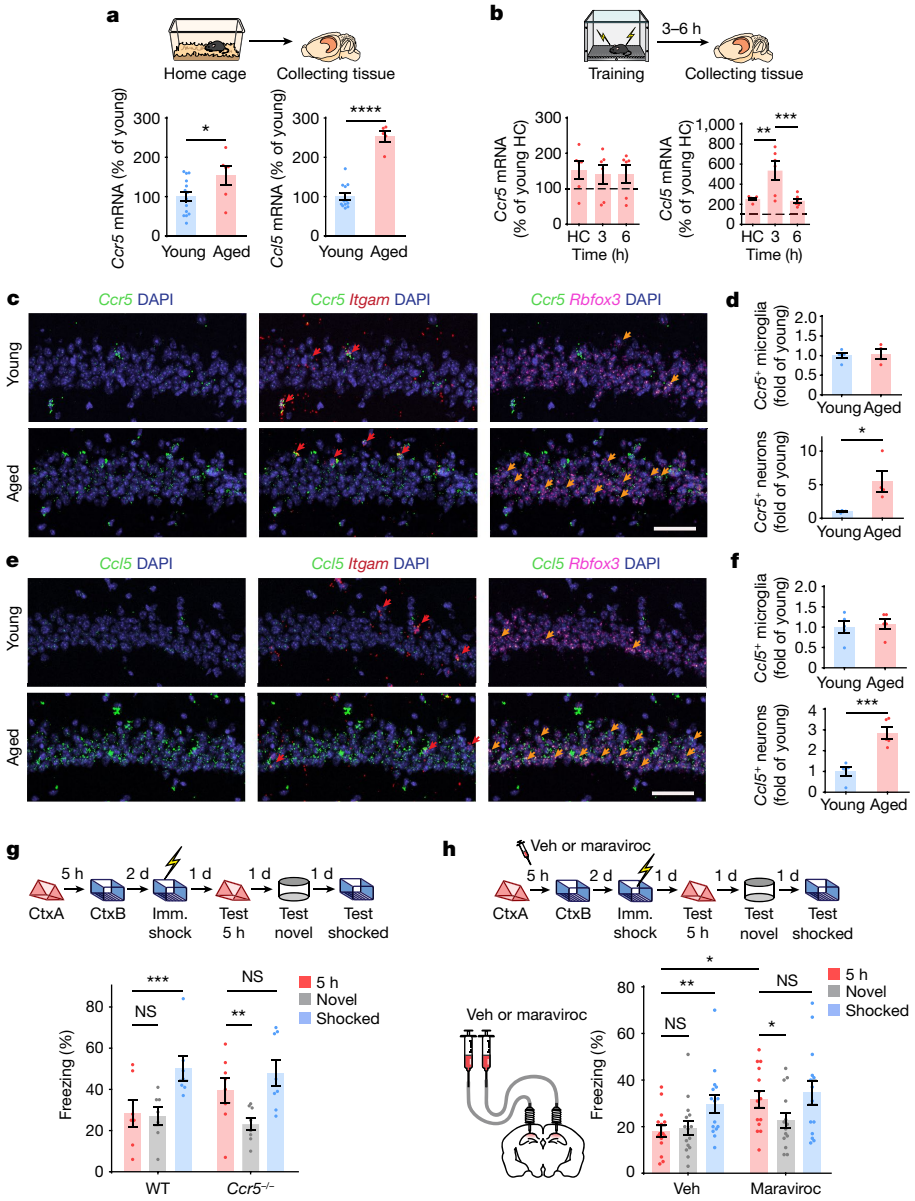

Fig. 4 | Enhanced CCL5–CCR5 signalling contributes to age-related memory linking deficits. a, Middle-aged home cage mice had higher mRNA levels of *Ccr5* and *Ccl5* in dCA1 than young home cage mice (*Ccr5*: young $n = 14$, aged $n = 6$ mice, *Ccl5*: young $n = 12$, aged $n = 5$; $^{*}P < 0.05$, $^{****}P < 0.0001$, Student's *t*-test). **b**, *Ccr5* and *Ccl5* expression after fear conditioning in dCA1 of middle-aged mice (*Ccr5*: $n = 6$ mice for all groups, *Ccl5*: HC $n = 5$, 3 h n = 6, 6 h $n = 6$; $^{**}P < 0.01$, $^{***}P < 0.001$, one-way ANOVA). **c**, Representative images of *Ccr5*, *Itgam* and *Rbfox3* mRNA expression in dCA1 from naive young or middle-aged mice. Red arrows: cells expressing *Ccr5* and *Itgam*. Orange arrows: cells expressing *Ccr5* and *Rbfox3*. Scale bar, 50 µm. **d**, Number of *Ccr5*-expressing microglia and neurons in young or middle-aged mice (young $n = 5$, aged $n = 4$ mice; $^{*}P < 0.05$, Student's *t*-test). **e**, Representative images of *Ccl5*, *Itgam* and *Rbfox3* mRNA expression in dCA1 from naive young or middle-aged mice. Red arrows: cells expressing *Ccr5* and *Itgam*. Orange arrows: cells expressing *Ccr5* and *Rbfox3*. Scale bar, 50 µm. **f**, Number of *Ccl5*-expressing microglia and neurons in young or middle-aged mice ($n = 5$ mice; $^{***}P < 0.001$, Student's *t*-test). **g**, *Ccr5* knockout rescued 5-h memory linking deficits in middle-aged mice (WT $n = 7$, $Ccr5^{-/-}$ $n = 8$ mice; $^{**}P < 0.01$, $^{***}P < 0.001$, two-way repeated measures ANOVA). **h**, Maraviroc, a CCR5 antagonist, rescued 5-h memory linking deficits in middle-aged mice (veh $n = 15$, maraviroc $n = 14$ mice; $^{*}P < 0.05$, $^{**}P < 0.01$, two-way repeated measures ANOVA). All results are shown as mean ± s.e.m.

(shRNA-mediated knockdown and a knockout) extended the temporal window for memory linking. Similar to $Ccr5^{-/-}$ mice, *Ccl5* knockout ($Ccl5^{-/-}$) mice also showed an extended linking window (Extended Data Fig. 6g), indicating that CCL5 is critical for CCR5 regulation of memory linking. To test whether CCR5 regulates linking for other forms of memory, we developed a memory linking task based on place preference with saccharin water used as a reward (Extended Data Fig. 6a). As with contextual memory linking with fear conditioning, the mice were able to link two memories when they were separated by five hours but not by seven days (Extended Data Fig. 6b–d). In addition, infusing CCL5 into dCA1 also inhibited memory linking in this appetitive linking task tested with a five-hour interval, providing evidence that activation of CCR5 inhibits both forms of memory linking (Extended Data Fig. 6e, f).

Altogether, our results show that increasing or inhibiting CCR5 signalling impairs or extends (respectively) the temporal window for contextual memory linking, thus confirming that CCR5 has a key role in setting the duration for the memory linking window.

CCR5 modulates memory co-allocation

Next, we investigated how CCR5 regulates the temporal window for contextual memory linking. Previous results suggested that a temporary increase in neuronal excitability after learning[25,26] biases the allocation of a subsequent memory to the neuronal ensemble that encodes the initial memory[1], and that this ensemble overlap was critical for memory linking[27]. Thus, we examined whether CCR5 modulated neuronal excitability and consequently memory ensemble overlap, as this could explain the role of CCR5 in shaping the temporal window for memory linking. When treated with CCL5, dCA1 neurons from acute hippocampal slices showed a decrease in current-injection-induced firing rate (Fig. 3a, b), indicating an inhibition of neuronal excitability. This is an important result, as neuronal excitability is critical for determining which specific neurons in a neural network will store a given memory (known as memory allocation)[13,18,28]. Notably, decreases in excitability, caused by increases in CCR5 signalling following learning, could explain how this receptor decreases memory ensemble overlap, and thus closes the window for memory linking.

To directly test whether increases in CCR5 activity could decrease memory allocation, Opto-CCR5-EGFP or the EGFP control were expressed in mouse dCA1, and then subjected to blue light for 30 min (at different light power levels) before context exploration (Fig. 3c). After light activation (4 and 8 mW) and contextual training, dCA1 neurons expressing Opto-CCR5 showed a significant reduction in the expression of learning-induced c-Fos, a widely used marker for neurons involved in memory[29] (Fig. 3d, e), whereas the overall number of c-Fos$^+$ or EGFP cells was similar among groups (Extended Data Fig. 7g, h). This result supports the hypothesis that activation of CCR5 excludes neurons from memory ensembles. In addition, light activation did not cause any changes in c-Fos expression in the EGFP$^+$ cells in the EGFP control group (Extended Data Fig. 7c–f). Furthermore, when AAV8 containing shRNA against *Ccr5* was injected into dCA1, neurons with *Ccr5* knockdown had a higher probability of expressing c-Fos (that is, being involved in memory; Extended Data Fig. 7a, b) compared with control neurons, a result that also supports the hypothesis that CCR5 activity modulates memory allocation in neuronal networks.

Altogether, the results presented suggest that the increase in CCR5 expression and signalling after learning prevents subsequent memories from being allocated to the neuronal ensemble encoding the initial memory, thus reducing the overlap between the two memory ensembles, and consequently attenuating memory linking. To test this hypothesis, we first labelled the memory neural ensembles activated by two contextual exposures with the cFos-tTA/TRE-mCherry system and with *Fos* mRNA in situ hybridization (*Fos* encodes c-Fos). There was significantly higher expression of *Ccr5* in the non-overlapping neuronal ensemble population than in the overlapping population, and there was a negative correlation between *Ccr5* expression in cells encoding the first contextual memory and the probability of overlap between the two memory ensembles (Fig. 3f–h), indicating that increased *Ccr5* expression in the first memory engram reduces the overlap between the two memory ensembles.

To further test this hypothesis, we recorded neuronal calcium activity (with GCaMP6f) in dCA1 with head-mounted fluorescent microscopes (miniscopes[1]) while mice were exploring two different contexts separated by five hours, one day, two days or seven days. We then measured the overlap between the active neuronal populations recorded during the two contextual exposures in both wild-type and *Ccr5* knockout mice (Fig. 3i, j). Compared to wild-type mice, *Ccr5*$^{-/-}$ mice exhibited an overall significantly higher neural ensemble overlap (Fig. 3k). Neurons in a contextual memory ensemble were reported to have a significantly higher mean firing rate[30]. Therefore, we next focused our analyses on the cells with high (top 10%) activity during the contextual exposures. There was a time-dependent reduction in the neuronal activity of this group of cells with high activity in wild-type mice, whereas no reduction was observed in *Ccr5*$^{-/-}$ mice (Extended Data Fig. 8). When the overlap between high-activity cells was measured, a time-dependent (five hours versus two days) decrease in overlap was observed in wild-type mice, and this decrease was attenuated by the *Ccr5* knockout (Extended Data Fig. 9). Altogether these results support the hypothesis that CCR5 modulates the temporal window for memory linking by regulating neuronal co-allocation and consequently the overlap between memory ensembles.

CCR5 and ageing-related linking deficits

CCR5 and CCL5 expression in peripheral immune cells increases with age[31,32]. Similar increases in ageing neurons could contribute to age-related decreases in contextual memory linking[1]. To test this hypothesis, we measured hippocampal expression of *Ccr5* and *Ccl5* in mice aged around 16–18 months (middle-aged), an age at which mice still show intact contextual conditioning, but deficits in contextual memory linking[1]. Compared with young mice, middle-aged home cage mice had significantly enhanced levels of *Ccl5* and *Ccr5* mRNA (Fig. 4a). Middle-aged mice also showed an increase in the transient *Ccl5* expression at three hours after contextual learning (Fig. 4b), which was earlier than in young mice (6–12 h after learning; Fig. 1c). In situ hybridization showed that the increase in *Ccr5* and *Ccl5* expression was mainly in neurons (Fig. 4c–f).

Although middle-aged wild-type mice showed deficits in contextual memory linking[1], even when short intervals (five hours) were used (Fig. 4g), middle-aged *Ccr5*$^{-/-}$ mice showed clear evidence for memory linking tested with a five-hour interval (higher freezing in contexts A than in a novel context; Fig. 4g). To test the effect of pharmacologically blocking CCR5 activity on contextual memory linking in middle-aged mice, maraviroc (an FDA-approved CCR5 antagonist used for HIV treatment[33]; Extended Data Fig. 4d–f) was infused to dCA1 of these mice one hour before they were exposed to context B in a contextual memory linking experiment with a five-hour interval. Unlike control mice, maraviroc-treated mice showed memory linking (Fig. 4h). Thus, blocking CCR5 with maraviroc ameliorates the memory linking deficits in middle-aged mice. Altogether these results suggest that CCR5 expression has a role in closing the temporal window for memory linking as well as in age-related deficits in memory linking.

In summary, our findings show that a delayed (12–24 h) increase in CCL5–CCR5 signalling in dCA1 neurons of a given memory ensemble closes the temporal window for memory linking. Activation of CCR5 decreases neuronal excitability, and thus negatively regulates memory allocation. This change in memory allocation decreases the overlap between memory ensembles, and therefore impairs the ability of one memory to trigger the recall of the other, thus closing the temporal window for memory linking (Extended Data Fig. 10). Notably, our findings also show that an age-related increase in CCL5–CCR5 expression leads to impairments in memory linking in middle-aged mice that can be reversed with an FDA-approved drug that inhibits this receptor—a result that could have substantial clinical implications. Together, our results provide the first insights into the molecular and cellular mechanisms that close the temporal window for memory linking, thus segregating the memories for events that are temporally distinct.

Online content

Any methods, additional references, Nature Research reporting summaries, source data, extended data, supplementary information, acknowledgements, peer review information; details of author contributions and competing interests; and statements of data and code availability are available at https://doi.org/10.1038/s41586-022-04783-1.

1. Cai, D. J. et al. A shared neural ensemble links distinct contextual memories encoded close in time. *Nature* **534**, 115–118 (2016).

2. Rashid, A. J. et al. Competition between engrams influences fear memory formation and recall. *Science* **353**, 383–387 (2016).
3. Abdou, K. et al. Synapse-specific representation of the identity of overlapping memory engrams. *Science* **360**, 1227–1231 (2018).
4. Yetton, B. D., Cai, D. J., Spoormaker, V. I., Silva, A. J. & Mednick, S. C. Human memories can be linked by temporal proximity. *Front. Hum. Neurosci.* **13**, 315 (2019).
5. Mack, M. L., Love, B. C. & Preston, A. R. Building concepts one episode at a time: The hippocampus and concept formation. *Neurosci. Lett.* **680**, 31–38 (2018).
6. Zhou, L. & Saksena, N. K. HIV associated neurocognitive disorders. *Infect. Dis. Rep.* **5**, e8 (2013).
7. Ellis, R., Langford, D. & Masliah, E. HIV and antiretroviral therapy in the brain: neuronal injury and repair. *Nat. Rev. Neurosci.* **8**, 33–44 (2007).
8. Jung, W. & Lee, S. H. Memory deficit in patients with schizophrenia and posttraumatic stress disorder: relational vs item-specific memory. *Neuropsychiatr. Dis. Treat.* **12**, 1157–1166 (2016).
9. Avery, S. N. et al. Impaired relational memory in the early stage of psychosis. *Schizophr. Res.* **212**, 113–120 (2019).
10. Czajkowski, R. et al. Encoding and storage of spatial information in the retrosplenial cortex. *Proc. Natl Acad. Sci. USA* **111**, 8661–8666 (2014).
11. Han, J. H. et al. Selective erasure of a fear memory. *Science* **323**, 1492–1496 (2009).
12. Sano, Y. et al. CREB regulates memory allocation in the insular cortex. *Curr. Biol.* **24**, 2833–2837 (2014).
13. Zhou, Y. et al. CREB regulates excitability and the allocation of memory to subsets of neurons in the amygdala. *Nat. Neurosci.* **12**, 1438–1443 (2009).
14. Lanfranco, M. F., Mocchetti, I., Burns, M. P. & Villapol, S. Glial- and neuronal-specific expression of CCL5 mRNA in the rat brain. *Front. Neuroanat.* **11**, 137 (2017).
15. Zhou, M. et al. CCR5 is a suppressor for cortical plasticity and hippocampal learning and memory. *eLife* **5**, e20985 (2016).
16. Torres-Muñoz, J. E., Van Waveren, C., Keegan, M. G., Bookman, R. J. & Petito, C. K. Gene expression profiles in microdissected neurons from human hippocampal subregions. *Brain Res. Mol. Brain Res.* **127**, 105–114 (2004).
17. Shepherd, A. J., Loo, L. & Mohapatra, D. P. Chemokine co-receptor CCR5/CXCR4-dependent modulation of Kv2.1 channel confers acute neuroprotection to HIV-1 glycoprotein gp120 exposure. *PLoS ONE* **8**, e76698 (2013).
18. Yiu, A. P. et al. Neurons are recruited to a memory trace based on relative neuronal excitability immediately before training. *Neuron* **83**, 722–735 (2014).
19. Lee, D. et al. Temporally precise labeling and control of neuromodulatory circuits in the mammalian brain. *Nat. Methods* **14**, 495–503 (2017).
20. Airan, R. D., Thompson, K. R., Fenno, L. E., Bernstein, H. & Deisseroth, K. Temporally precise in vivo control of intracellular signalling. *Nature* **458**, 1025–1029 (2009).
21. Shideman, C. R., Hu, S., Peterson, P. K. & Thayer, S. A. CCL5 evokes calcium signals in microglia through a kinase-, phosphoinositide-, and nucleotide-dependent mechanism. *J. Neurosci. Res.* **83**, 1471–1484 (2006).
22. Marozsan, A. J. et al. Mechanisms involved in stimulation of human immunodeficiency virus type 1 replication by aminooxypentane RANTES. *J. Virol.* **75**, 8624–8638 (2001).
23. Wang, S. W. et al. CCL5 and CCR5 interaction promotes cell motility in human osteosarcoma. *PLoS ONE* **7**, e35101 (2012).
24. Shen, W. et al. Activation of the chemotactic peptide receptor FPRL1 in monocytes phosphorylates the chemokine receptor CCR5 and attenuates cell responses to selected chemokines. *Biochem. Biophys. Res. Commun.* **272**, 276–283 (2000).
25. Moyer, J. R. Jr, Thompson, L. T. & Disterhoft, J. F. Trace eyeblink conditioning increases CA1 excitability in a transient and learning-specific manner. *J. Neurosci.* **16**, 5536–5546 (1996).
26. Oh, M. M., Oliveira, F. A. & Disterhoft, J. F. Learning and aging related changes in intrinsic neuronal excitability. *Front. Aging Neurosci.* **2**, 2 (2010).
27. Yokose, J. et al. Overlapping memory trace indispensable for linking, but not recalling, individual memories. *Science* **355**, 398–403 (2017).
28. Rogerson, T. et al. Molecular and cellular mechanisms for trapping and activating emotional memories. *PLoS ONE* **11**, e0161655 (2016).
29. Mayford, M. & Reijmers, L. Exploring memory representations with activity-based genetics. *Cold Spring Harb. Perspect. Biol.* **8**, a021832 (2015).
30. Tanaka, K. Z. et al. The hippocampal engram maps experience but not place. *Science* **361**, 392–397 (2018).
31. Mello, C. V. et al. Fat-storing multilocular cells expressing CCR5 increase in the thymus with advancing age: potential role for CCR5 ligands on the differentiation and migration of preadipocytes. *Int. J. Med. Sci.* **7**, 1–14 (2009).
32. Yung, R., Mo, R., Grolleau-Julius, A. & Hoeltzel, M. The effect of aging and caloric restriction on murine CD8+ T cell chemokine receptor gene expression. *Immun. Ageing* **4**, 8 (2007).

Methods

Mice

Ccr5 knockout (*Ccr5*$^{-/-}$) mice were purchased from Taconic Farms (B6.129P2-Ccr5tm1Kuz N10). Experimental wild-type, *Ccr5*$^{+/-}$ and *Ccr5*$^{-/-}$ mice (3 to 5 months old, both male and female) were generated by intercrossing *Ccr5*$^{+/-}$ mice. Littermates were used for the *Ccr5* knockout linking test. cFos-tTA mice that express tetracycline transactivator (tTA) protein under the control of the c-Fos (also known as Fos) promoter were maintained in a C57BL/6N background. *Ccrl5* knockout (*Ccl5*$^{-/-}$) mice were purchased from The Jackson Laboratory (B6.129 P2-Ccl5tm1Hso/J). Three-month-old to five-month-old male and female mice were used for the *Ccl5* knockout linking test. Sixteen-month-old male C57BL/6Nia were purchased from NIA for *Ccr5* expression detection and linking test. Eleven-week-old male C57BL/6N Tac mice were purchased from Taconic Farms for all other experiments. Mice are housed in an AAALAC accredited facility with 12 h–12 h light–dark cycles. Housing conforms to *The Guide for the Care and Use of Laboratory Animals*, 8th edition. The temperature setpoint is 72 degrees plus or minus 3 degrees; the humidity range is between 30% and 70%. All experiments were performed during the light phase of the cycle. Across experiments, mice were randomly assigned to experimental vs control groups in behavioural training, anatomical, optogenetic and miniscope studies with matched age and sex, whenever possible. All experimental protocols were approved by the Chancellor's Animal Research Committee of the University of California, Los Angeles, in accordance with NIH guidelines.

Viral constructs

Constructs for the *i*Tango2 system were gifts from H. Kwon; these include pAAV-hSYN-DRD2-V2tail-TevN-BLITz1-TetR-VP16-bGHpA (Addgene plasmid 89874; http://n2t.net/addgene:89874; RRID:Addgene_89874), pAAV-hSYN-bArrestin2-TevC-P2A-TdTomato-WPRE-bGHpA (Addgene plasmid 89873; http://n2t.net/addgene:89873; RRID:Addgene_89873), pAAV-TRE-EGFP (Addgene plasmid 89875; http://n2t.net/addgene:89875; RRID: Addgene_89875) and pTRE-EGFP (Addgene plasmid 89871; http://n2t.net/addgene:89871; RRID: Addgene_89871). pGP-CMV-NES-jRGECO1a was a gift from D. Kim and the GENIE Project (Addgene plasmid 61563; http://n2t.net/addgene:61563; RRID: Addgene_61563). pAAV.Syn.GCaMP6f.WPRE.SV40 was a gift from D. Kim and the GENIE Project (Addgene viral prep 100837-AAV1; http://n2t.net/addgene:100837; RRID:Addgene_100837). For the AAV-based shRNA construct for mouse CCR5, the target sequence (shCCR5) is 5′-GTGCAAGCTCAGTCTATACCTCAAGAGGGTATAGACTGAGCTTG CAC-3′. Thecontrol sequence (shDsRed) is 5′- AGTTCCAGTACGGCTC CAAGAAGCTTGTTGGAGCCGTACTGGAACT-3′. For the Opto-CCR5 experiment, pLenti-Ef1α-DIO-Opto-CCR5-EGFP was made by replacing the intracellular loops of rhodopsin with those of CCR5 to activate its specific intracellular signalling with light. Detailed viral information is provided in Supplementary Table 1.

Quantitative PCR

Total RNA was prepared using the RNeasy Mini Kit (Qiagen, 74104) according to the manufacturer's instructions. Single-stranded cDNA was synthesized using SuperScript III First-Strand Synthesis SuperMix (Invitrogen, 18080400). Quantitative PCR (qPCR) was performed with SYBR Green-based reagents (iQ SYBR Green Supermix; Bio-Rad, 1708880) using a LightCycler 480 II (Roche). The following are primers used for qPCR: mouse *Ccr5*, 5′-GCTGCCTAAACCCTGTCATC-3′ and5′-GTTCTCCTGTGGATCGGGTA-3′;mouse*Ccl5*,5′-TGCAGTCGTGT TTGTCACTC-3′ and5′-AGAGCAAGCAATGACAGGGA-3′;mouse *Ccl3*, 5′-TTCCACGCCAATTCATCGTT-3′ and5′-GCATTCAGTTCCAGGTCAGTG-3′;mouse*Ccl4*,5′-CCTCCCACTTCCTGCTGTTT-3′and 5′-GCTTGGAG CAAAGACTGCTG-3′;mouse *36B4* (also known as *Rplp0*) 5′-AGATGCA GCCAGATCCGCAT-3′ and 5′-GTTCTTGCCCATCAGCACC-3′.

In situ hybridization

Mouse brains were dissected and fast-frozen in optimal cutting temperature compound (OCT) by dry ice without paraformaldehyde (PFA) fixation. Twenty-micrometre frozen sections were sliced. In situ hybridization was performed using the RNAscope Fluorescent Multiplex Reagent Kit V1(ACD, 320850) and V2 (ACD, 323120) according to the manufacturer's instructions. RNAscope Probe-Mm-*Ccr5* (ACD, 438651) and Probe-Mm-*Ccl5* were used to detect *Ccr5* and *Ccl5* mRNA. Probe-Mm-*Rbfox3* (ACD, 313311) and Probe-Mm-*Itgam* (ACD, 469601) were used as markers for neurons and microglia, respectively. Probe-Mm-*Slc17a7* (ACD, 416631) and Probe-Mm-*Gad2* (ACD, 311491) were used as markers for excitatory and inhibitory neurons. Probe-*mCherry* (ACD, 431201) and Probe-Mm-*Fos* (316921) were used for memory ensemble labelling.

Immunostaining

Mice were transcardially perfused with 4% PFA (4% paraformaldehyde in 0.1 M phosphate buffer) and after perfusion, brains were sliced coronally (50 μm thick) with a vibratome and processed for immunostaining. Primary antibodies, including chicken polyclonal anti-GFP (Abcam AB13970, 1:1,000), mouse monoclonal anti-GFP (Synaptic Systems, 132 011, 1:500), chicken anti-RFP (Synaptic Systems, 409 006, 1:500), mouse anti-TetR monoclonal antibody (Clone 9G9, Takara, 63113, 1:500), mouse anti-NeuN (Chemicon, MAB377, 1:1,000), rabbit anti-GFAP (Dako, Z0334, 1:500), rabbit anti-c-Fos (Cell Signaling, 9F6, 2250, 1:500) and rabbit anti-P2Y12 (AnaSpec, AS-55043A, 1:1,000) and secondary antibodies, including goat anti-chicken 488 (Invitrogen, A11039, 1:2,000), goat anti-mouse 488 (Invitrogen, A11029, 1:2,000), goat anti-chicken 594 (Invitrogen, A11042, 1:2,000) and goat anti-rabbit 647 (Invitrogen, A21245, 1:2,000) were used for immunostaining. Brain slices were incubated with 4′,6-diaminodino-2-phenylindole (DAPI; Invitrogen, 1:2,000) for 10 min and washed with PBS three times before mounting onto slides. Immunostaining images were acquired by NIS-Elements AR (Nikon, v.4.40.00) with a Nikon A1 Laser Scanning Confocal Microscope (LSCM). NIS-Elements AR Analysis (Nikon, v.4.40.00) was used to analyse the confocal images.

Immunoblotting

Cultured HEK293 cells were lysed with RIPA buffer (Sigma, R0278) with protease inhibitor cocktail (Sigma, P8340), phosphatase inhibitor cocktail 2 (Sigma, P5726) and phosphatase inhibitor cocktail 3 (Sigma, P0044). Protein samples (10 μg per well) were loaded to NuPAGE Novex 4–12% Bis-Tris protein gel (Thermo Fisher Scientific, NP0336BOX) and transferred onto polyvinylidene difluoride (PVDF) membranes. The membranes were then blocked with 5% non-fat milk at room temperature for 1 h and then probed with primary antibodies (phospho-p44/42 MAPK, Cell Signaling 9101, 1:4,000 dilution) at 4 °C overnight. Membranes were then incubated with HRP-conjugated secondary antibodies (goat anti-rabbit HRP, Bio Rad, 170–6515, 1:5,000) for 1 h and developed with SuperSignal solutions (Thermo Fisher Scientific). Then the membrane was stripped and probed again with primary antibodies (p44/42 MAPK, Cell Signaling 9102, 1:4,000 dilution, β-actin 1:10,000, A5316, Sigma-Aldrich) and secondary antibodies including goat anti-mouse HRP (Bio Rad, 170–6516, 1:10,000) and goat anti-rabbit HRP (Bio Rad, 170–6515, 1:5,000).

CCR5-*i*Tango2 system

The inducible Tango2 (*i*Tango2) system is a genetic method of labelling and manipulating cells with particular GPCR activation[19]. On the basis of this method, we designed CCR5-*i*Tango2. In brief, it couples a tetracycline-controlled transcriptional activator (tTA) to the C terminus of mouse CCR5 via a specific tobacco etch virus protease (TEVp)-sensitive cleavage site (TCS), which is protected by AsLOV2/Jα (light-sensitive domain). After activation, β-arrestin tagged with TEVp-C

(C-terminal region of TEVp) binds the intracellular loop of CCR5 tagged with TEVp-N (N-terminal region of TEVp), which forms functional TEVp and cleave TCS after AsLOV2/Jα/TCS complex was exposed to light stimulation. Then tTA is released and translocates into the nucleus to induce specific gene expression. To generate the CCR5-*i*Tango2 DNA constructs, full-length mouse CCR5 cDNA was subcloned into pAAV-hSYN-DRD2-V2tail-TevN-BLITz1-TetR-VP16-bGHpA to replace DRD2 cDNA sequence (by VectorBuilder).

For analysis, ImageJ (v.1.53f51) was used to quantify the EGFP and tdTomato intensity. In brief, EGFP cells were identified and outlined automatically (to create ROIs for $EGFP^+$ counting) by threshold imaging (threshold: 1.5-fold of the background intensity). Then, the intensity (grey value) of the EGFP and tdTomato was measured by the software within the ROIs of identified cells, and the EGFP/tdTomato ratio was calculated.

Opto-CCR5 system

Opto-XR is a genetically encoded optical tool[20] that can control GPCR-initiated biochemical signalling pathways with high spatiotemporal precision. On the basis of opto-XR, the laboratory of W.D.H. designed and made the Opto-CCR5 construct and subcloned it into a lentivirus backbone (Lenti-Ef1a-DIO-Opto-CCR5-EGFP). In brief, the intracellular loops of rhodopsin were replaced with those of mouse CCR5. As a result, a light-induced structure change of rhodopsin would activate intracellular CCR5 signalling.

Stereotaxic surgery

Mice were anaesthetized with 2% isoflurane and placed in a stereotaxic head frame on a heat pad. Artificial tears were applied to the eyes to prevent eye drying. A midline incision was made down the scalp, and a craniotomy was performed with a dental drill. After surgery, the mice were subcutaneously injected with carprofen (5 mg kg^{-1}) and dexamethasone (0.2 mg kg^{-1}) before recovery. Water with amoxicillin was applied for two weeks.

For cannula implantation, two guide cannulas (Plastics One, C313GS-5/SPC) were implanted at the following coordinates relative to bregma (mm): (1) for dCA1, AP: −2.1, ML: ±1.7; (2) for lateral ventricle, AP: −0.3, ML: ±1.0. Three weeks after cannulation, mice were anaesthetized and sterilized vehicle or drug was infused into hippocampus through the internal cannula (Plastics One, C313IS-5/Spc, 100 nl min^{-1}) at DV: −1.6 mm (dCA1) or −2.5 mm (ventricle) relative to the skull. After infusion, the internal cannula was left in place for an additional 5 min to ensure full diffusion. Drugs with the following concentration were infused: mouse CCL5 peptide (70 nM in PBS, 1 μl), maraviroc (10 mg ml^{-1} in saline with 7.5% beta-cyclodextrin, 1 μl), DAPTA (50 nM in PBS, 1 μl).

For virus injection, a Nanoliter injector (World Precision Instruments) was used to infuse virus with Micro4 Controller (World Precision Instruments). Virus was infused at 50–100 nl min^{-1}. After infusion, the capillary was kept at the injection site for 5 min and then withdrawn slowly. The incision was closed with clips, which were removed 7 days later. Details of the viruses used are provided in Supplementary Table 1.

For optical fibre implantation, fibre Optic Cannula (Newdoon, 200 μm, NA = 0.37) was immediately implanted after virus injection. The tip of the optic fibre was placed 600 μm above the virus injection site. Then, the canula was fixed with Metabond and dental cement.

For miniscope implantation, a GRIN lens was implanted into the dorsal hippocampal CA1 region as previously described[1]. After GCaMP6f virus injection, an approximately 2-mm-diameter circular craniotomy was centred at the injection site. The cortex directly below the craniotomy was aspirated with a 27-gauge blunt syringe needle attached to a vacuum pump. Cortex buffer (NaCl 135 mM, KCL 5 mM, $CaCl_2$ 2.5 mM, $MgSO_4$ 1.3 mM, HEPES 5mM, pH 7.4) was repeatedly applied to the exposed tissue to prevent drying. The GRIN lens (0.50 NA, 2.0 mm in diameter, Grintech Gmbh) was slowly lowered above CA1 to a depth of 1.35 mm ventral to the surface of the skull at the most posterior point of the craniotomy. Next, a skull screw was used to anchor the lens to the skull. Both the lens and the skull screw were fixed with superglue (Loctite, 45198) and dental cement (Jet Denture Repair Package, Lang, 1223CLR). Low Toxicity Silicone Adhesive (Kwik-Sil, World Precision Instruments) was used to cover the GRIN lens for protection. Three weeks later, a small baseplate was cemented onto the mouse's head on top of the previously formed dental cement.

Memory ensemble labelling with cFos-tTA mice

Adult male and female (3–8 months old) cFos-tTa transgenic mice were bilaterally microinjected with 500 nl of AAV1-TRE-mCherry into dCA1. Mice were allowed to recover from surgeries for 3 weeks and high-doxycycline chow (1 g kg^{-1}) was applied during the recovery. Mice were removed from doxycycline chow and were fed with regular chow for 3 days before the behaviour to allow the tagging of neuronal ensemble for the memory linking experiments. The activity-dependent tagging was shut off by administration of high-doxycycline chow 1 h after behavioural tagging.

Optogenetics

For the CCR5-*i*Tango2 system, 3 weeks after virus injection and optic cannula implantation, the mice were handled for 3 days and then habituated with the optic fibre connected in their home cage for another 3 days (10 min per day). Then the mice received contextual fear conditioning training and were returned to their home cage. After 2.5 h, 5.5 h, 11.5 h and 23.5 h, different groups of mice received light stimulation in their home cage (473 nm, 8–10 mW, 10 s on/50s off for 1 h). The mice were kept for another 48 h for GFP expression before the brains were collected and fixed with PFA perfusion. To validate CCR5-*i*Tango2 in vitro, HEK293 cells were transfected with *i*Tango2 system constructs using Lipofectamine 2000 (Invitrogen, 11668027). One day later, light (473 nm, 10 s on/50 s off for 1 h) was delivered to the cells with or without CCL5 (1 nM).

For Opto-CCR5, the mice were anaesthetized with 1.5% isoflurane during light delivery (473 nm, around 8 mW, 50 s on/10 s off for 30 min). Then the mice were returned to their home cage for 30 min to recover before exposure to a different context. To validate Opto-CCR5 in vitro, HEK293 cells were transfected with the Opto-CCR5 construct using Lipofectamine 2000 (Invitrogen, 11668027). One day later, light (473 nm or 500 nm, around 1–2 mW mm^{-2}, 2–5 min) was delivered to the cells to activate Opto-CCR5.

For memory ensembles labelling with $ChR2_{ETTC}$ (an ultrafast and sensitive version of ChR2) pre-activation, 3 weeks after virus injection and optic cannula implantation, the mice were handled for 3 days (2 min per day) and then habituated to the experimental room and wearing optical fibres for another 3 days. For the pre-activation, mice were connected to the optical fibres and returned to their home cages for 5 min first, and then 3 min light stimulation (473 nm, around 4–5 mW, 10 Hz, 20% duty cycle) was applied in the home cage. After light stimulation, optical fibres were disconnected and mice were allowed another 5 min recovery in their home cage before contextual fear conditioning.

Memory linking with contextual fear conditioning

The contextual memory linking task was performed as previously described[1]. Mice were first handled for 3days (1 min per day) and then habituated to transportation and external environmental cues for 2 min in the experimental room each day for another 3 days. In the contextual memory linking task, mice explored two different contexts (A and then B, counterbalanced) which were separated by 5 h–7 days. Mice explored each context for 10 min. For immediate shock, mice were placed in chamber B for 10 s followed by a 2-s shock (0.65 mA). At 58 s after the shock, mice were placed back in their home cage. For the context tests, mice were returned to the designated context. Freezing was assessed using an automated scoring system (Med Associates) with 30 frames per second sampling; the mice needed to freeze continuously for at least 1 second before freezing could be counted.

Memory linking with place preference task

Mice were gradually water restricted to 1.5–2.0 ml per day. Body weight was tightly monitored every day to avoid a loss of over 15% of body weight. From the third day of water restriction, mice were handled for 5 min per day for 3 days. Then mice were placed in the experimental room for 1 h per day for another 3 days for habituation. To test memory linking, mice were exposed to one of the two-compartment apparatus (context A or context B, for each group the two contexts were counter balanced) for 10 min, and 5 h or 7 days later, mice were placed in context C (with 1.5 ml water containing 0.2% saccharin) for 15 min. One day later, mice were placed back in the two-compartment apparatus and were allowed to freely explore context A (pre-exposed context) and context B (novel context). The exploration was recorded and the time in each apparatus was measured to examine the preference for each context.

Slice preparation and CCL5 treatment

Adult mice (3–6 months old) were deeply anaesthetized with isoflurane and the brains were rapidly dissected out and transferred to oxygenated (95% O_2/5% CO_2), ice-cold cutting solution containing 92 mM NaCl, 2.5 mM KCl, 1.25 mM NaH_2PO_4, 30 mM $NaHCO_3$, 20 mM HEPES, 25 mM glucose, 2 mM thiourea, 5 mM sodium ascorbate, 3 mM sodium pyruvate, 2 mM $CaCl_2$, and 2 mM $MgCl_2$. Coronal slices (400 μm thick) containing the hippocampus were cut using a Leica VT1200 vibrating blade microtome, transferred to a submerged holding chamber containing oxygenated cutting solution and allowed to recover for 1 h at room temperature. Before whole-cell recordings were performed, each slice was incubated in a separate chamber containing either oxygenated artificial cerebrospinal fluid (aCSF) (containing 115 mM NaCl, 10 mM glucose, 25.5 mM $NaHCO_3$, 1.05 mM NaH_2PO_4, 3.3 mM KCl, 2 mM $CaCl_2$, and 1 mM $MgCl_2$) or 10 nM CCL5 in oxygenated aCSF for 1h. After incubation, slices were immediately transferred to a superfused recording chamber and constantly perfused with oxygenated aCSF maintained at 28 °C. All recordings were performed within 30 min of aCSF or CCL5 incubation.

Whole-cell patch recordings

Whole-cell current–clamp recordings were performed on pyramidal neurons in the CA1 region of the hippocampus using pipettes (3–5 MΩ resistance) pulled from thin-walled borosilicate glass using a Sutter P97 Flaming/Brown micropipette puller and filled with an internal solution containing 120 mM potassium methyl sulfate, 10 mM KCl, 10 mM HEPES, 10 mM sodium phosphocreatine, 4 mM magnesium ATP and 0.4 mM sodium GTP. All recordings were obtained using a MultiClamp 700B amplifier controlled by the pClamp 10 software and digitized using the Digidata 1440A system. Signals were filtered at 10 kHz and digitized at 20 kHz. Neurons were included in the study only if the initial resting membrane potential (V_m) was less than −55 mV and the access resistance (R_a) was less than 20 MΩ, and were rejected if the R_a changed by more than 20% of its initial value. For all recordings, neurons were held at −65 mV. The stable resting membrane potential of neurons was measured and averaged over a 60-s duration with 0-mA current injection immediately after breaking in. To investigate the firing rate of neurons, the number of action potentials fired in response to a 600-ms pulse of depolarizing current injection (0 pA to 380 pA in 20-pA increments) was calculated. Three pulses were delivered for each current amplitude and the average number of action potentials fired for each current amplitude was plotted. The recordings were analysed using Stimfit 0.15.8 and the data were screened for statistical outliers (±2 s.d.).

Miniscope data acquisition and analyses

One-photon calcium imaging was recorded using UCLA miniscopes[34]. During recordings, digital imaging data were sent from the CMOS imaging sensor (Aptina, MT9V032) to custom data acquisition (DAQ) electronics and USB Host Controller (Cypress, CYUSB3013) over a lightweight, highly flexible co-axial cable. Images were acquired at 30 frames per second, using display resolution at 752 × 480 pixels (1 pixel = 1–2 μm), and saved into uncompressed avi files. The analysis pipeline was written in MATLAB using first the NoRMCorre algorithm for motion correction (rigid registration)[35], followed by individual neuron identification and extraction using the CNMF-E algorithm[36]. During motion correction, videos were 2× spatially downsampled using the default built-in NoRMCorre protocol. During CNMF-E initialization, videos were further 2× spatially downsampled and 5× temporally downsampled. The quality of neuron extraction was verified using a MATLAB custom-made Neuron Deletion GUI. We excluded the detected putative neurons exhibiting ROI morphology or calcium trace abnormalities or incoherencies between the calcium trace peaks and the expected correspondent fluorescence increases in the video, and the neuron deletion was performed by experimenters blinded to the experimental groups and conditions. Each 10-min video from individual sessions was analysed separately. Recordings from multiple sessions of the same mouse were aligned using the spatial footprints (neuron.A, output from CNMF-E) of each one of the detected cells for individual sessions. The centroid distance and spatial correlation were calculated for all cell pairs. Cell pairs from different sessions were considered to match if their spatial correlation was at least 0.8 and their centroid distance was 5 pixels or less. Overlapping percentages between two given sessions were calculated as the number of matched cells over the average of the total number of detected cells in each one of the two sessions. Overlapping index = Ctx A^+ Ctx B^+ cell (Overlap)/[(Ctx A^+ cell + Ctx B^+ cell)/2] %.

We reanalysed our miniscope data using a MATLAB custom-made concatenation analysis pipeline[37] to identify, track and analyse the activity of individual neurons across sessions. In brief, the motion-corrected videos (as described above), from context exposure sessions of individual mice, were aligned and concatenated into a long video. The long video was then processed through CNMF-E using the same parameters described above to extract putative neurons. After deletion of false-positive ROIs using the Neuron Deletion GUI protocol described above, we projected the raw calcium trace of the remaining ROIs for each session separately using the CNMF-E algorithm. Finally, we inferred spike activity from raw calcium traces from individual sessions using the Foopsi Thresholded algorithm[38], and we binarized neuronal activity (NA) from individual frames into 1 (active frame) and 0 (inactive frame). We calculated interevent intervals (IEI) as the time interval between consecutive active frames from individual sessions (Extended Data Fig. 8). The cumulative distribution of IEIs was first calculated for each individual neuron, then averaged across neurons to represent individual mice. Finally, the single mouse values were averaged to depict group results (Extended Data Fig. 8c, d, g). We defined subsets of neurons on the basis of their average NA by calculating the number of active frames for each neuron within specific sessions and sorting cells from highest to lowest NA (for example, top 10%, as in Extended Data Fig. 9b) or from lowest to highest NA (for example, bottom 10%, as in Extended Data Fig. 9c). The coefficient of variation for each neuron in a specific session was defined as the ratio between the standard deviation of the IEI distribution and the average NA within that session. We validated the usage of IEI from calcium imaging as a significantly reliable representation of inter-spike interval (ISI) from in vivo electrophysiology recordings (ephys) by leveraging a dataset containing simultaneous GCaMP6f calcium imaging and loose-seal cell-attached electrical recordings of cortical neuronal activity[39]. ISIs were defined as the time interval between consecutive spikes and the coefficient of variation for ephys recordings was calculated the same way as in calcium imaging recordings using the ISI distribution instead of the IEI distribution.

We defined the probability of overlap based on average NA by calculating the probability of a subset of neurons from Ctx A (for example,

top 10% NA) to have a specific relative level of NA (for example, be within the top 30% NA) in Ctx B. This was mathematically defined as in the example: $P_{A10,B30} = \frac{N_{A10,B30}}{U}$, where $P_{A10,B30}$ is the probability of the top 10% NA in Ctx A (A10) being within the top 30% NA in Ctx B (B30); $N_{A10,B30}$ is the actual number of neurons lying within A10 and B30; and U is the universe of all cells detected from all sessions by the analysis using the concatenated long video. The probability values were normalized by chance through the calculation of the ratio between $P_{A10,B30}$ and $P_{A10} \times P_{B30}$ (= 0.1 × 0.3) (Extended Data Fig. 9b–d). For plots in Extended Data Fig. 9b, c (*x* axis), the same percentage values were used for contexts A and B (for example, $P_{A10,B10}$, $P_{A20,B20}$,...). We have also calculated $P_{A10,B10}$ between different subsets of 10% cells from Ctx A and the top 10% NA cells from Ctx B (Extended Data Fig. 9e). We have spanned all cells from Ctx A, from highest to lowest NA, with a sliding window of size = 10% and step = 2% (Extended Data Fig. 9e, *x* axis). To express the significance of the probability of overlap values, they were represented as standard deviations from the mean of a null distribution created by randomly subsampling (10,000 times) 10% cells from Ctx A followed by the calculation of $P_{A10,B10}$, in which B10 is the top 10% NA from Ctx B.

Colocalization calculation

Different calculations were applied to reflect colocalization between protein or mRNA distributions. For overlap between c-Fos and Opto-CCR5/ChR2$_{ETTC}$/CCR5-*i*Tango2/shCCR5, chance level = (c-Fos$^+$/DAPI) × (EGFP$^+$/DAPI)%, colocalization = [(c-Fos$^+$EGFP$^+$/DAPI)%/Chance level]%, distribution index = [a/(a + b)]%, a = (c-Fos$^+$EGFP$^+$/EGFP$^+$)%, b = (c-Fos$^+$EGFP$^-$/EGFP$^-$)%, EGFP$^+$, c-Fos$^+$ and EGFP$^+$ indicate the number of cells with positive signal, respectively. Opto-CCR5, CCR5-*i*Tango2 and shCCR5 had EGFP as the reporter, whereas ChR2$_{ETTC}$ was tagged with mCherry instead. For overlap among *Ccr5*, *mCherry* and *Fos* mRNA, overlapping probability (over chance) = (a − b)/b, a = (*mCherry*$^+$*Fos*$^+$/DAPI)% (which is the observed overlap %), b = [(*mCherry*$^+$/DAPI) × (*Fos*$^+$/DAPI)]% (which is the overlap chance %).

Statistics and reproducibility

The investigators who collected and analysed the data including behaviour, miniscope, electrophysiological and staining were blinded to the mouse genotypes and treatment conditions. Error bars in the figures indicate the s.e.m. All statistical analyses were performed using GraphPad Prism 6. For behaviour experiments, *n* designates the number of mice. For biochemical experiments, *n* designates the number of brains or cells collected. For electrophysiological measurements, *n* designates the number of neurons. All statistical tests are two-sided. Statistical significance was assessed by Student's *t*-test, Kolmogorov–Smirnov test or one- or two-way ANOVA where appropriate, followed by the indicated post-hoc tests for repeated measures. Significance levels were set to $P = 0.05$. Significance for comparisons: $^*P < 0.05$; $^{**}P < 0.01$; $^{***}P < 0.001$. Detailed statistical information is provided in Supplementary Table 2.

Representative histological images were repeated independently in different mice with similar results for Fig. 1d ($n \geq 4$ per group), Fig. 1h ($n = 3$ per group), Fig. 1i ($n \geq 5$ per group), Fig. 2d, f ($n = 6$), Fig. 3c ($n \geq 3$ per group), Fig. 3f ($n = 6$), Fig. 4c ($n \geq 4$ per group) and Fig. 4e ($n = 5$ per group), and Extended Data Fig. 1e ($n \geq 3$ per group), Extended Data Fig. 1e ($n \geq 3$ per group), Extended Data Fig. 1g ($n = 5$ per group), Extended Data Fig. 2a ($n = 5$), Extended Data Fig. 2d ($n = 4$), Extended Data Fig. 2h ($n = 4$ per group), Extended Data Fig. 3l ($n \geq 3$ per group), Extended Data Fig. 4b ($n = 3$ per group), Extended Data Fig. 4e ($n \geq 3$ per group), Extended Data Fig. 4h ($n \geq 4$ per group) Extended Data Fig. 5f ($n = 4$), Extended Data Fig. 7a ($n = 8$) and Extended Data Fig. 7d ($n = 4$ per group). Representative in vitro images were biologically duplicated.

Reporting summary

Further information on research design is available in the Nature Research Reporting Summary linked to this paper.

Data availability

The original videos and datasets generated and/or analysed during the current study are available from the corresponding authors.

Code availability

The code for concatenation analysis of miniscope videos is available on GitHub.
https://github.com/Almeida-FilhoDG/ConcatMiniscope. All other code is available from the corresponding authors.

33. Wilkin, T. J. & Gulick, R. M. CCR5 antagonism in HIV infection: current concepts and future opportunities. *Annu. Rev. Med.* **63**, 81–93 (2012).
34. Aharoni, D., Khakh, B. S., Silva, A. J. & Golshani, P. All the light that we can see: a new era in miniaturized microscopy. *Nat. Methods* **16**, 11–13 (2019).
35. Pnevmatikakis, E. A. & Giovannucci, A. NoRMCorre: an online algorithm for piecewise rigid motion correction of calcium imaging data. *J. Neurosci. Methods* **291**, 83–94 (2017).
36. Zhou, P. et al. Efficient and accurate extraction of in vivo calcium signals from microendoscopic video data. *eLife* **7**, e28728 (2018).
37. Almeida-Filho, D. ConcatMiniscope: This is the first release of the ConcatMiniscope Pipeline (v.1.0.0-Beta). *Zenodo* https://doi.org/10.5281/zenodo.5676164 (2021).
38. Friedrich, J., Zhou, P. & Paninski, L. Fast online deconvolution of calcium imaging data. *PLoS Comput. Biol.* **13**, e1005423 (2017).
39. Wei, Z. et al. A comparison of neuronal population dynamics measured with calcium imaging and electrophysiology. *PLoS Comput. Biol.* **16**, e1008198 (2020).

Acknowledgements We thank A. Macalino, E. Chen, E. Ramirez, C. Riviere-Cazaux, M. López-Aranda and E. Lu for advice and technical support; M. Sehgal and L. M. De Biase for providing transgenic mice; and A. Luchetti for analysis discussion. This work was supported by grants from the NIMH (R01 MH113071), NIA (R01 AG013622) and NINDS (R01 NS106969), and from the Dr. Miriam and Sheldon G. Adelson Medical Research Foundation to A.J.S.

Author contributions Y.S. and M.Z. contributed to experimental design, data acquisition and analyses, and drafting and revising the article. D.C. performed memory linking time course experiments and memory linking in aged *Ccr5* knockout mice. G.F. performed electrophysiology experiments. Y.C. and Y.S. performed qPCR experiments. N.K. and W.D.H. made the Opto-CCR5 construct. J.L. and W.D.H. made the Tre-mCherry construct. M.K. produced lentivirus with the Opto-CCR5 construct. A.F.d.S. did memory linking in *Ccl5* knockout mice. D.N., C.Z., A. Liu, X.K., S.L., S.S., M.T. and T.S. helped with data acquisition. D.A.F., A. Lavi and S.H. helped with data analyses and interpretation. A.J.S. contributed to experimental design and interpretation, drafting and revising the article.

Competing interests The authors declare no competing interests.

Additional information

Supplementary information The online version contains supplementary material available at https://doi.org/10.1038/s41586-022-04783-1.

Correspondence and requests for materials should be addressed to Miou Zhou or Alcino J. Silva.

Peer review information *Nature* thanks Kaoru Inokuchi and the other, anonymous, reviewer(s) for their contribution to the peer review of this work. Peer reviewer reports are available.

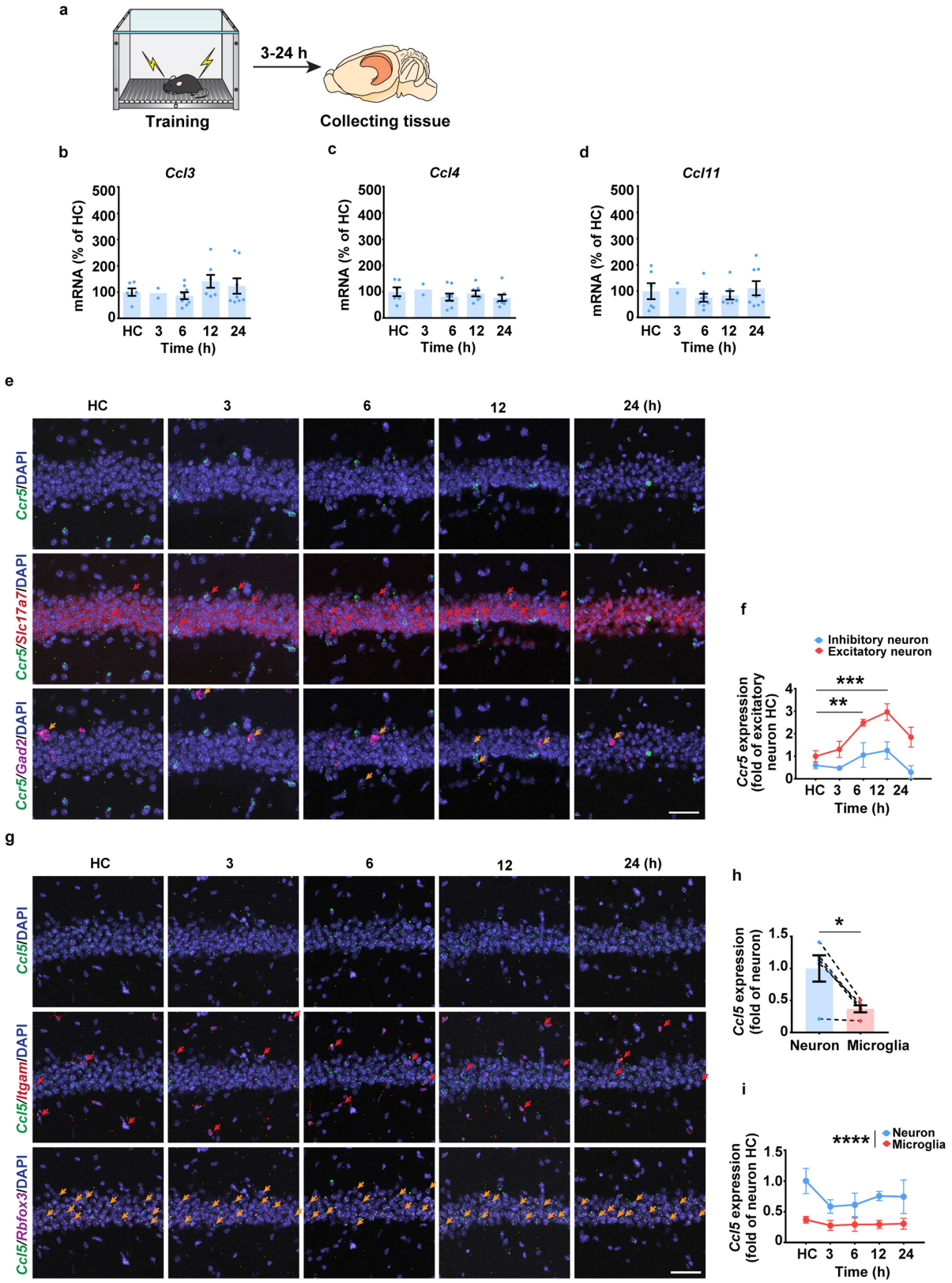

Extended Data Fig. 1 | See next page for caption.

Extended Data Fig. 1 | Dorsal hippocampal expression of CCR5 and its ligands after fear conditioning. a, Schematics of hippocampal tissue collection. **b**-**d**, qPCR experiment to measure *Ccl3* (**b**), *Ccl4* (**c**), and *Ccl11* (**d**) expression in naïve mice (HC) and in mice at different times after contextual fear conditioning. HC=home cage. HC n = 6, 3 h n = 2, 6 h n = 8, 12 h n = 7, 24 h n = 8 mice. **e**, Representative images of *Ccr5*, *Slc17a7* (excitatory neuronal marker), and *Gad2* (inhibitory neuronal marker) mRNA expression in dCA1 from naïve mice or mice 3–24 h after fear conditioning. Red arrows: cells expressing *Ccr5* and *Slc17a7*. Orange arrows: cells expressing *Ccr5* and *Gad2*. Scale bar, 50 µm. **f**, Number of *Ccr5*-expressing excitatory and inhibitory neurons 3–24 h after fear conditioning (HC n = 4, 3 h n = 4, 6 h n = 4, 12 h n = 4, 24 h n = 3 mice; $^{**}P < 0.01$, $^{***}P < 0.001$, two-way repeated measures ANOVA). **g**, Representative images of *Ccl5*, *Itgam*, and *Rbfox3* mRNA expression in dCA1 from naïve mice or mice 3–24 h after fear conditioning. Red arrows: cells expressing *Ccl5* and *Itgam*. Orange arrows: cells expressing *Ccl5* and *Rbfox3*. Scale bar, 50 µm. **h**, Number of *Ccl5*-expressing microglia and neurons in naïve mice (n = 5 mice; $^{*}P < 0.05$, paired t-test). **i**, Number of *Ccl5*-expressing microglia and neurons in HC mice and 3–24 h after fear conditioning (n = 5 mice per group; $^{****}P < 0.0001$, two-way repeated measures ANOVA). All results shown as mean ± s.e.m.

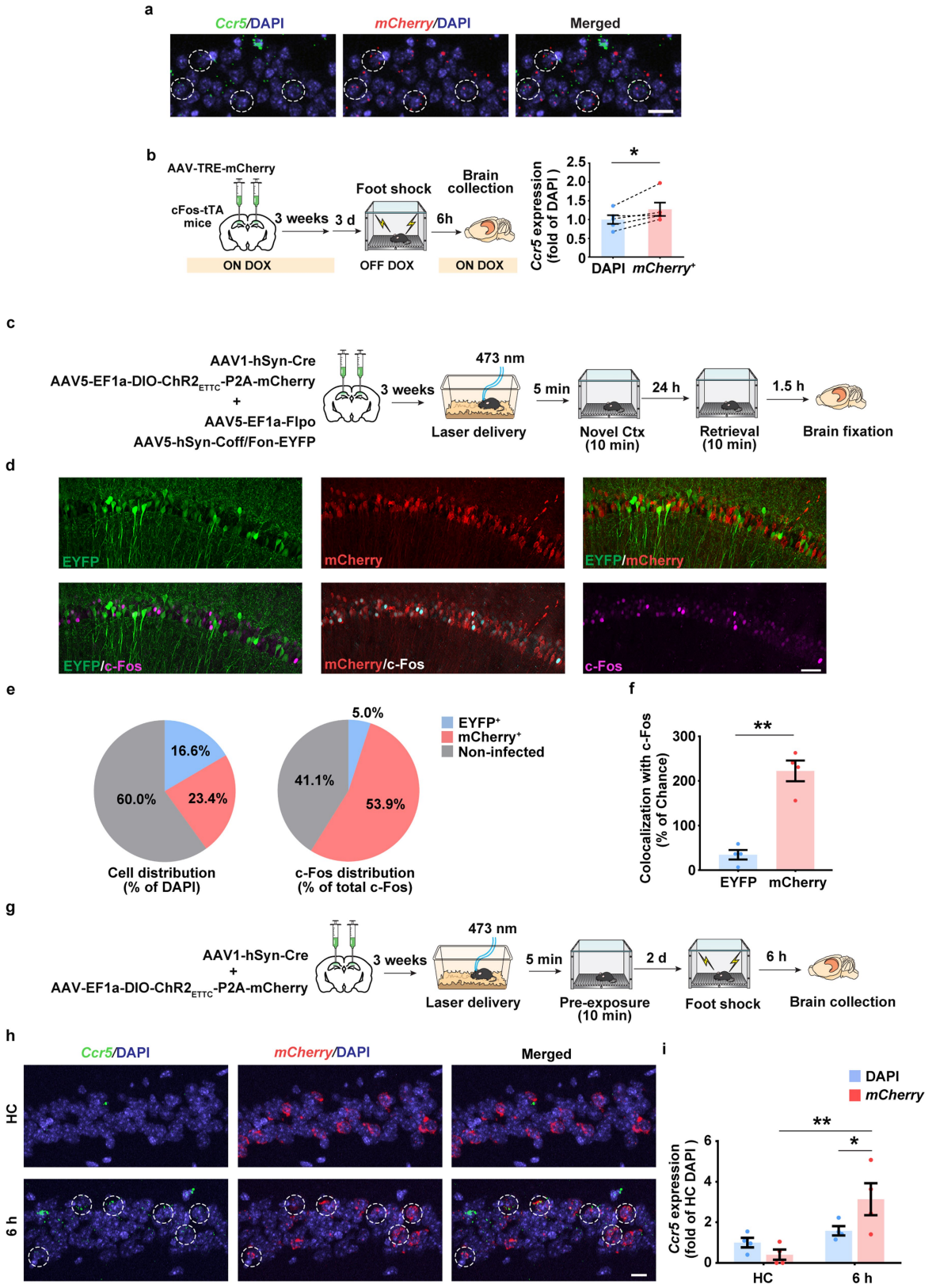

Extended Data Fig. 2 | See next page for caption.

Extended Data Fig. 2 | The colocalization of *Ccr5* expression and memory ensembles measured with cFos-tTA mice and the optogenetic ($ChR2_{ETTC}$) pre-activation system. a, Representative images of *Ccr5* and *mCherry* (neuronal ensemble) mRNA expression in dCA1 from cFos-tTA mice 6h after fear conditioning. Colocalization was labelled with dashed circles. Scale bar, 20 μm. **b**, Quantification of *Ccr5* expression in total cells (DAPI) and neuronal ensemble (*mCherry*$^+$). (n = 5 mice; $^*P < 0.05$, paired t-test). **c**, Schematics to use blue light to activate $ChR2_{ETTC}$-expressing neurons to be involved in neuronal ensemble by pre-activation. INTRSECT system (Cre-off/Flp-on) was used to label non-$ChR2_{ETTC}$-expressing neurons as the control. **d**, Representative images of mCherry (pre-activated neurons), c-Fos (neuronal ensembles), and EYFP (non-preactivated neurons) in dCA1 24h after the novel context exposure. Scale bar, 50 μm. **e**, c-Fos distribution in mCherry$^+$, EYFP$^+$ or non-infected cells. **f**, Quantification of the colocalization between c-Fos and mCherry or EYFP. Colocalization (of c-Fos and mCherry) = (c-Fos$^+$mCherry$^+$/DAPI)/[(c-Fos$^+$/DAPI)*(mCherry$^+$/DAPI)] (n = 4 mice per group; $^{**}P < 0.01$, paired Student's t-test). **g**, Schematics to detect the colocalization of *Ccr5* expression in neuronal ensembles using pre-activation system. **h**, Representative images of *Ccr5* and *mCherry* (pre-activated neuronal ensemble) mRNA expression in dCA1 6h after fear conditioning. Colocalization was labelled with dashed circles. Scale bar, 20 μm. **i**, Quantification of *Ccr5* expression in total cells (DAPI) and pre-activated neuronal ensemble (*mCherry*$^+$) (n = 4 mice per group; $^*P < 0.05$, $^{**}P < 0.01$, two-way repeated measures ANOVA). All results shown as mean ± s.e.m.

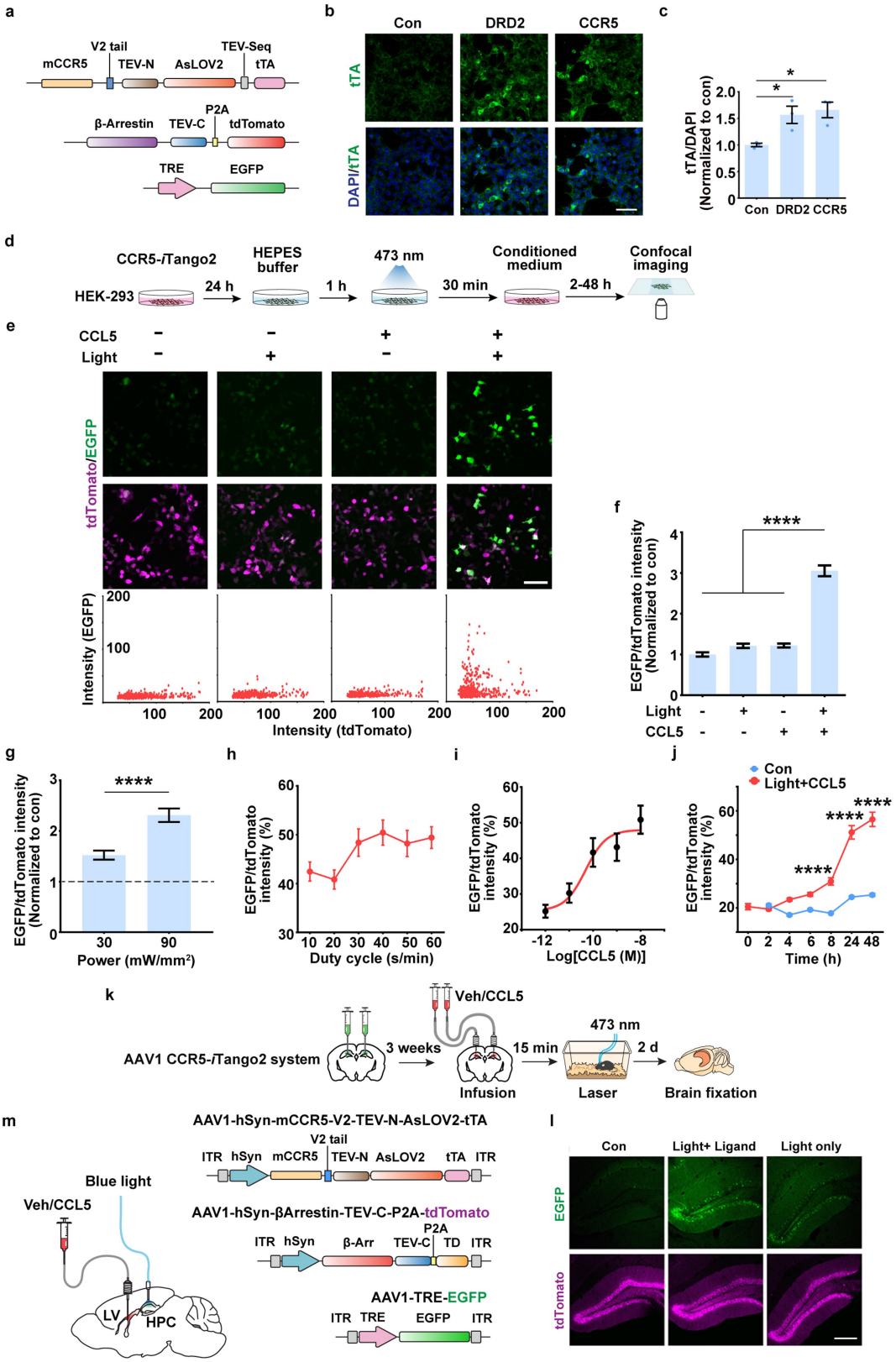

Extended Data Fig. 3 | See next page for caption.

Extended Data Fig. 3 | Characterization of CCR5-*i*Tango2. a, Schematics of CCR5-*i*Tango2 constructs. **b**, **c**, Expression validation of the CCR5-*i*Tango system in HEK-293 cells. DRD2-*i*Tango2 (for Dopamine 2 receptor) was used as a positive control. **b**, Representative images of tTA immunostaining. Scale bar, 50 µm. **c**, Quantification of tTA expression (intensity normalized to DAPI). n = 3 slides per group; $^{*}P < 0.05$, one-way ANOVA. **d**, HEK-293 cells were transfected with 3 plasmids (see methods) for 24h and then treated with 10 nM CCL5 and blue light to induce EGFP expression. **e**, Representative images of EGFP expression after different treatments. Light^{-}CCL5^{-} n = 558, Light^{+}CCL5^{-} n = 507, Light^{-}CCL5^{+} n = 521, Light^{+}CCL5^{+} n = 500 cells. Scale bar, 50 µm. **f**, Quantification of EGFP and tdTomato ratio (intensity). Compared to control, light or CCL5 group, only the group with both light and CCL5 showed EGFP expression. Light^{-}CCL5^{-} n = 70, Light^{+}CCL5^{-} n = 97, Light^{-}CCL5^{+} n = 97, Light^{+}CCL5^{+} n = 282 cells; $^{****}P < 0.0001$, one-way ANOVA. **g**, Power-dependent EGFP expression. Results were normalized to no light control (30 mW/mm^2 n = 320, 90 mW/mm^2 n = 307 cells; $^{****}P < 0.0001$, student's t-test). **h**, Duty cycle dependent EGFP expression. The light stimulation was delivered every minute (~0.017 Hz) to induce EGFP expression. Light was kept on for 10–60 s during each stimulation to induce EGFP expression (10 s/min n = 407, 20 s/min n = 377, 30 s/min n = 307, 40 s/min n=383, 50 s/min n = 353, 60 s/min n = 524 cells). **i**, Dose curve of CCL5 to induced CCR5 activation (measured by EGFP/tdTomato fluorescence ratio) in cultured HEK-293 cells (10^{-12} M n = 49, 10^{-11} M n = 39, 10^{-10} M n = 29, 10^{-9} M n = 77, 10^{-8} M n = 86 cells). **j**, Time course of EGFP expression. The green fluorescence increased monotonically during the different time intervals investigated. Compared to other time intervals (2, 4, 6, 8 and 24 h), the 48h time interval showed the highest EGFP/tdTomato ratio (Light^{+}CCL5^{+} 0 h n = 58, 2 h n = 194, 4 h n = 282, 6 h n = 310, 8 h n = 316, 24 h n = 396, 48 h n = 345 cells; Light^{-}CCL5^{-} 2 h n = 195, 4 h n = 219, 6 h n = 290, 8 h n = 304, 24 h n = 445, 48 h n = 401 cells; $^{****}P < 0.0001$, two-way ANOVA). **k**, Schematics of CCR5-*i*Tango2 AAVs injected into mouse hippocampus and validated through intra-hippocampal infusion of CCL5 and fiber-optic light stimulation. **l**, Representative images of CCR5-*i*Tango2-expressing hippocampal dentate gyrus neurons in control condition (no light and CCL5), light only, and light with CCL5. Ligand and light were directly delivered into the hippocampus. Scale bar, 250 µm. **m**, Left: To test CCR5-*i*Tango2 activation in dCA1 (Fig. 1h), CCL5 was infused into the lateral ventricle (LV) while light was delivered into dCA1 of hippocampus (HPC). Right: Schematics of CCR5-*i*Tango2 AAVs. All results shown as mean ± s.e.m.

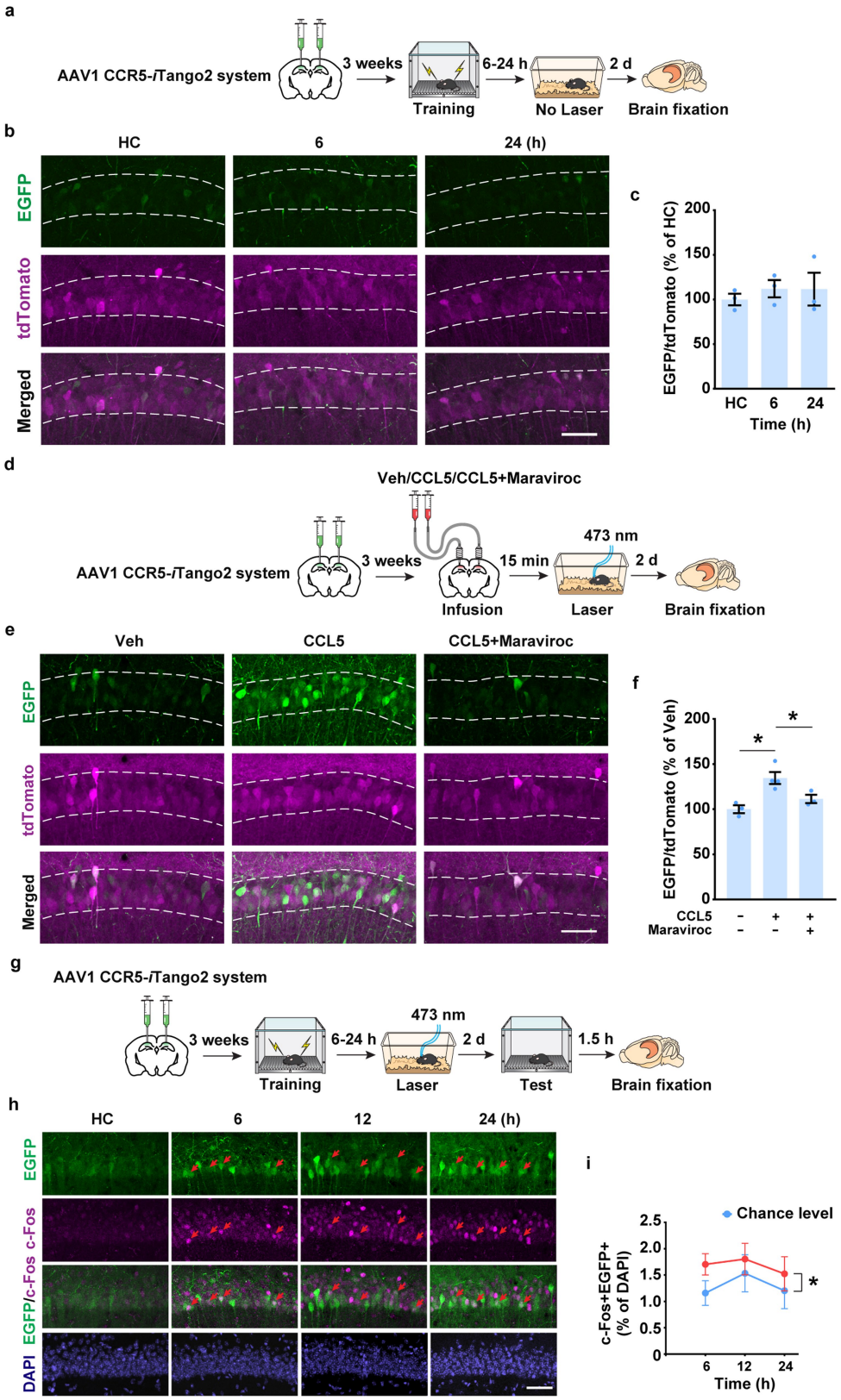

Extended Data Fig. 4 | See next page for caption.

Extended Data Fig. 4 | CCR5 activation measured with the CCR5-*i*Tango2 system in vivo. a–**c**, Validation of the leakage in CCR5-*i*Tango2 system in vivo. **a**, Schematics to test the CCR5-*i*Tango2 system without light activation. **b**, Representative images of EGFP and CCR5-*i*Tango2-expressing dCA1 neurons after fear conditioning. Scale bar, 50 µm. **c**, Quantification of EGFP expression (intensity normalized to tdTomato, n = 3 mice per group). **d**–**f**, Validation of the maraviroc mediated CCR5 inhibition in vivo. **d**, Maraviroc was co-infused with CCL5 into mouse dCA1. The CCR5-*i*Tango2 was used to measure CCR5 activation in vivo. **e**, Representative images of CCR5-*i*Tango2-expressing dCA1 neurons after fear conditioning. Scale bar, 50 µm. **f**, Quantification of EGFP expression in different treatment ($CCL5^-Maraviroc^-$ n = 3, $CCL5^+Maraviroc^-$ n = 4, $CCL5^+Maraviroc^+$ n = 3 mice; $^*P < 0.05$, one-way ANOVA). **g**–**i**, Analyses of colocalization of c-Fos and CCR5 activation in vivo. **g**, Schematics to test c-Fos expression in $EGFP^+$ cells after learning with the CCR5-*i*Tango2 system. **h**, Representative images of colocalization between EGFP and c-Fos in dCA1. Red arrows: $c\text{-}Fos^+EGFP^+$ cells. Scale bar, 50 µm. **i**, Percentage of $c\text{-}Fos^+EGFP^+$ cells in total cells (6 h n = 6, 12 h n = 4, 24 h n = 5 mice; $^*P < 0.05$, two-way repeated measures ANOVA). All results shown as mean ± s.e.m.

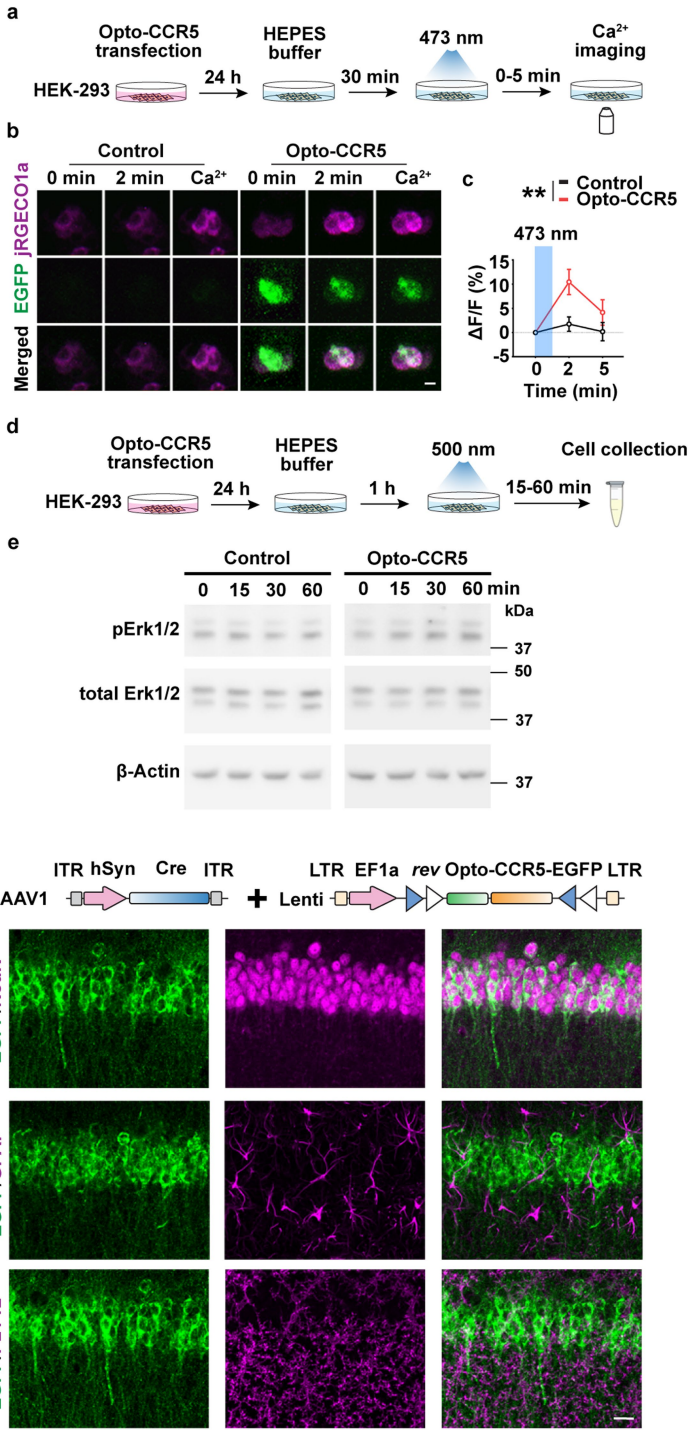

Extended Data Fig. 5 | Characterization of Opto-CCR5. a, HEK-293 cells were transfected with Opto-CCR5 and jRGECO1a (Calcium sensor with red florescence) for 24h and then stimulated with blue light to induce a calcium response. **b**, Representative images at 0 min or 2 min after stimulation, or in the medium with high calcium concentration. Scale bar, 20 μm. **c**, Quantification of florescence change after light stimulation. In HEK-293 cells, Opto-CCR5-EGFP activation by light significantly increased intracellular Ca^{2+} concentration reflected by jRGECO1a (Control 2 min n = 95, Control 5 min n = 96, Opto-CCR5 2 min n = 86, Opto-CCR5 5 min n = 89 cells; $^{**}P < 0.01$, two-way ANOVA). **d**, **e**, Opto-CCR5 activation increased pErk1/2 in HEK-293 cells. **d**, HEK-293 cells were transfected with the Opto-CCR5 construct. After 24h expression, the cells were starved in HEPES buffer for 1h before a 2 min light stimulation to reduce basal pErk1/2 levels. Cells were collected at 0 (no light stimulation), 15, 30 or 60 min after light stimulation and subjected to western blot analysis to investigate the phosphorylation level of Erk1/2 (**e**). **f**, Expression of Opto-CCR5 in dCA1 neurons. To express Opto-CCR5 in dCA1 neurons, AAV1-hSyn-Cre was co-injected with Lenti-DIO-Opto-CCR5. NeuN (neuron marker), GFAP (astrocyte marker) and P2Y12 (microglia marker) were co-stained with EGFP in dCA1. Scale bar, 20 μm. All results shown as mean ± s.e.m.

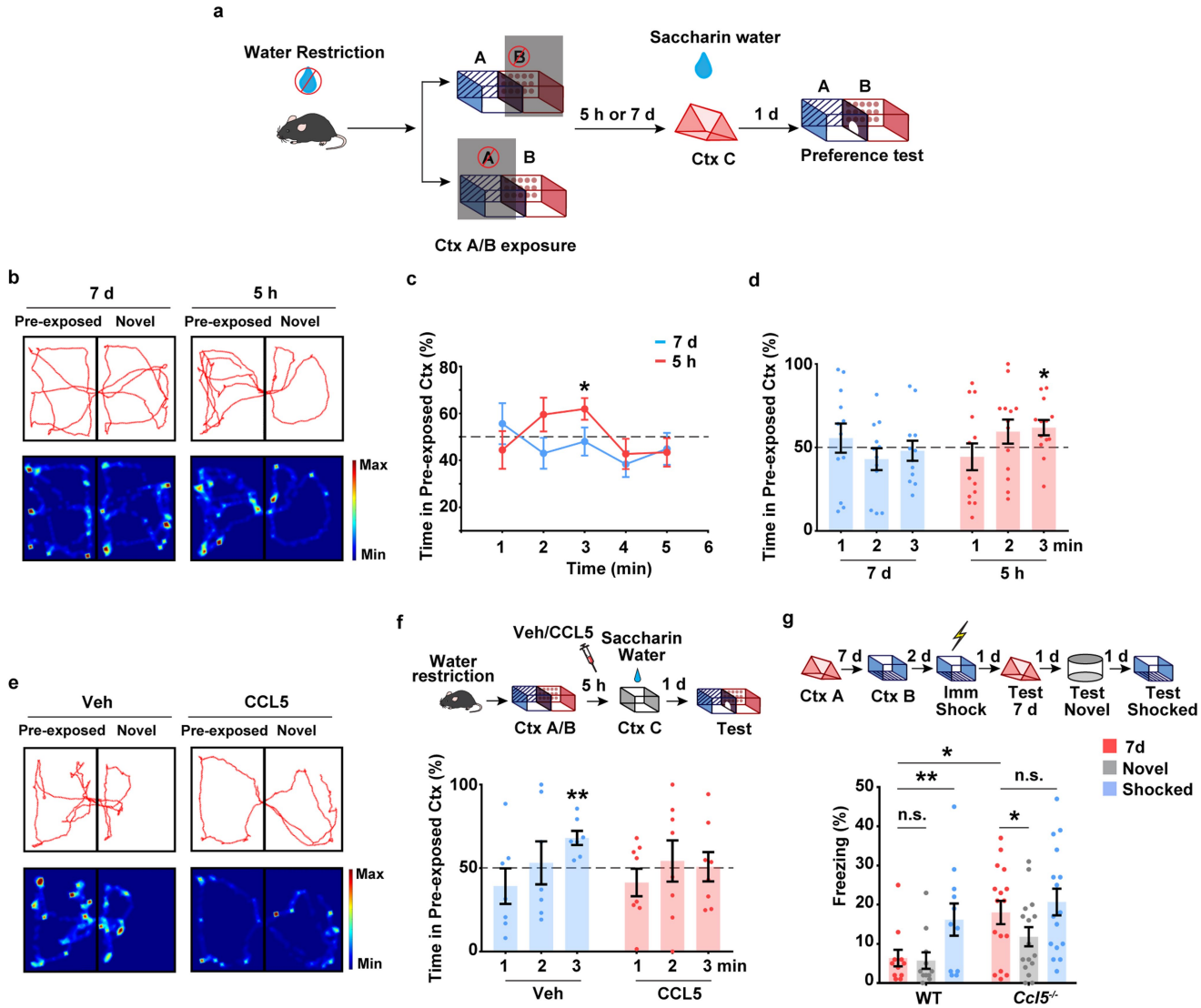

Extended Data Fig. 6 | CCR5/CCL5 signalling regulates memory linking in an appetitive place preference task. a–f, Place preference-based behaviour model to test the linking of contextual memories. **a**, Schematics of place preference-based linking behaviour. **b**, Representative trajectory plot (in the 3rd minute) of mice in the pre-exposed context and a novel context with a 5h and 7d interval. **c**, **d**, Mice showed a significant preference for pre-exposed context during the 3rd minute in the 5h group compared to the 7d group (5 h n = 13, 7d n = 12 mice; $^{*}P < 0.05$, one sample paired t-test compared to 50%). **e**, Representative trajectory plot (in the 3rd minute) of mice in the pre-exposed context and a novel context with Vehicle or CCL5 infusion. **f**, CCL5 infusion in dCA1 impaired contextual memory linking with a 5h interval (Veh n = 7, CCL5 n = 8 mice; $^{**}P < 0.01$, one sample paired t-test compared to 50%). **g**, *Ccl5* knockout extended the temporal window of contextual memory linking (WT n = 11, *Ccl5*$^{-/-}$ n = 16 mice; $^{*}P < 0.05$, $^{**}P < 0.01$, two-way repeated measures ANOVA). All results shown as mean ± s.e.m.

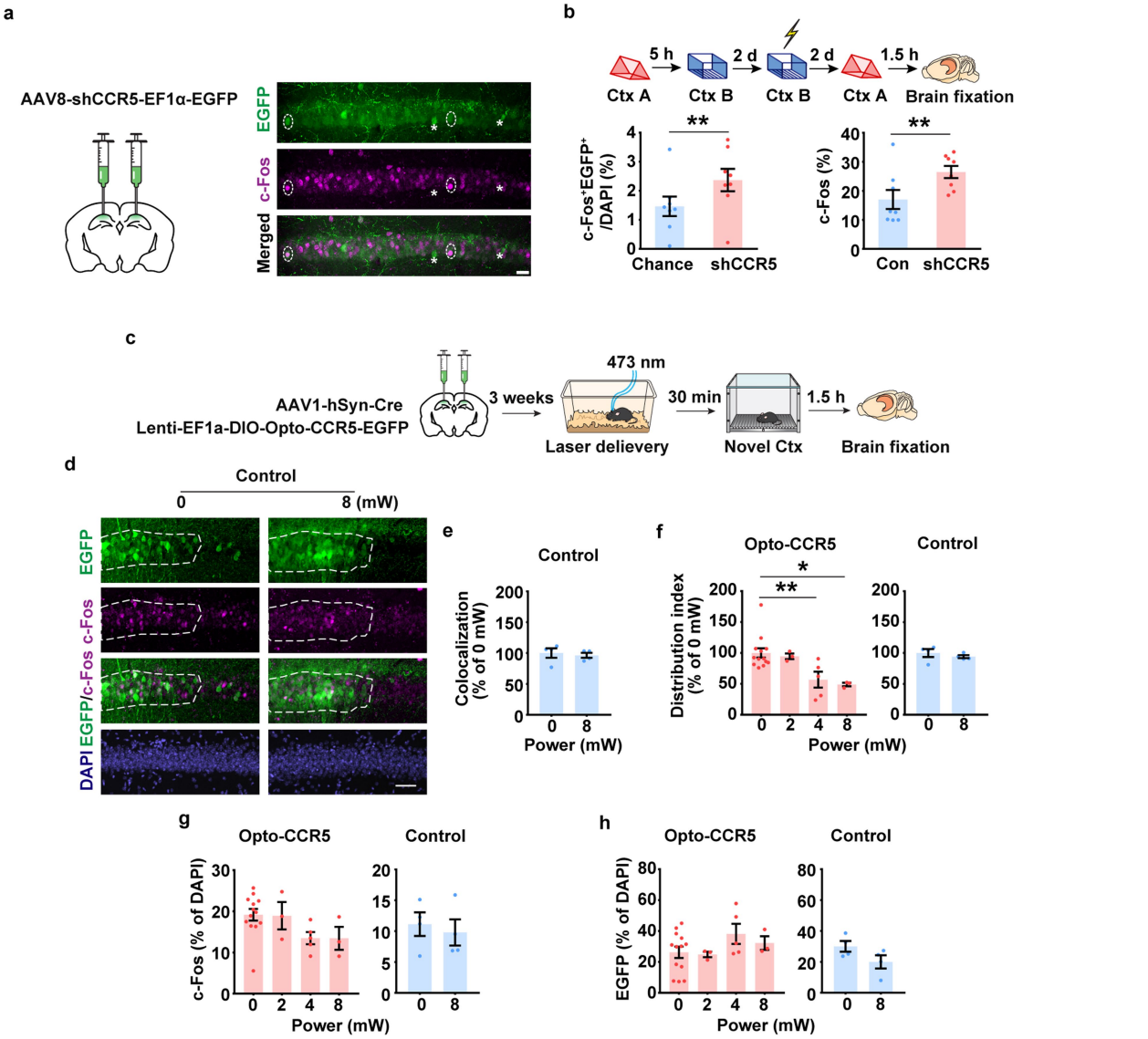

Extended Data Fig. 7 | CCR5 regulate memory allocation. a, **b**, *Ccr5* knockdown enhanced memory allocation. **a**, Schematics of AAV8-shRNA-CCR5-Ef1α-EGFP injection, and representative images of c-Fos and EGFP staining. Two EGFP$^+$c-Fos$^+$ cells were labelled by dotted line circle and two EGFP$^+$c-Fos$^-$ cells were labelled by asterisk. Scale bar, 20 μm. **b**, dCA1 neurons with *Ccr5* knockdown had a higher probability of expressing c-Fos after a memory test in context A. Left: The percentage of c-Fos$^+$EGFP$^+$ cells in total (DAPI). Right: percentage of c-Fos$^+$ cells in EGFP$^-$ cells (Con) or in EGFP$^+$ cells with *Ccr5* knockdown (shCCR5) (n = 8 mice, $^{**}P < 0.01$, paired t-test). **c**–**h**, Expression of c-Fos and Opto-CCR5 or EGFP control in dCA1 (Opto-CCR5 0 mW n = 13, 2 mW n = 3, 4 mW n = 5, 8 mW n = 3 mice; EGFP control n = 4 mice per group). **d**, Representative images of colocalization between c-Fos and EGFP control after light stimulation and novel context exposure. Scale bar, 50 μm. **e**, Colocalization between c-Fos$^+$ cells and EGFP$^+$ cells after normalization to chance level. **f**, Quantification of c-Fos distribution in EGFP$^+$ and EGFP$^-$ cells in the Opto-CCR5-EGFP or EGFP control group ($^*P < 0.05$, $^{**}P < 0.01$, one-way ANOVA). **g**, Percentage of c-Fos positive cells (normalized to cells with DAPI staining) in dCA1 with light stimulation of different power levels. **h**, Percentage of EGFP expression cells (normalized to cells with DAPI staining) in dCA1with light stimulation of different power levels. All results shown as mean ± s.e.m.

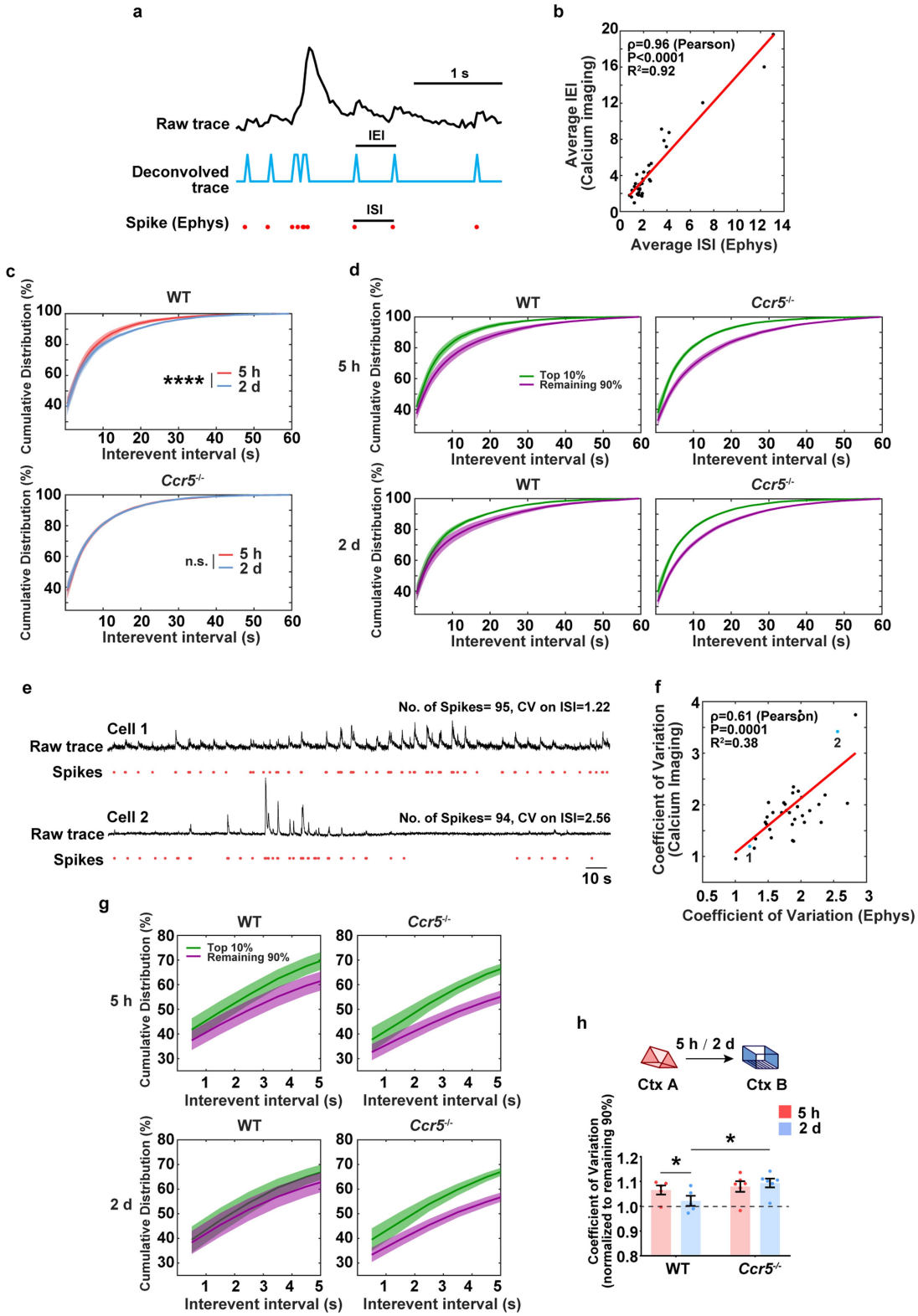

Extended Data Fig. 8 | See next page for caption.

Extended Data Fig. 8 | Analysis of the cumulative distribution of inter-event intervals recorded with miniscopes in wild-type and *Ccr5* knockout mice. a, Schematics used to extract spike information from raw traces of calcium imaging. Plot shows a 3s chunk of data from a single neuron using GCaMP6f calcium imaging and loose-seal cell-attached electrophysiological (Ephys) recordings. **b**, The average inter-event interval (IEI, from miniscope recordings) is highly correlated with the average inter-spike interval (ISI, by Ephys) (n = 36 cells; $R^2 = 0.92$, $P < 0.0001$, $\rho = 0.96$, Pearson's correlation coefficient). **c**, Cumulative distribution of IEI of the top 10% most active neurons (in Ctx A). The top 10% most active neurons from WT mice showed a significantly different distribution of IEI 5h compared to 2d after the context A exposure. In contrast, this subset of cells showed a similar pattern for both time intervals in *Ccr5*$^{-/-}$ mice (WT n = 5, *Ccr5*$^{-/-}$ n = 6 mice; ****$P < 0.0001$, Kolmogorov–Smirnov test). **d**, Cumulative distribution of IEIs of the top 10% most active neurons and the remaining 90% neurons (in Ctx A) at 5h or 2d after the context A exposure (WT n = 5, *Ccr5*$^{-/-}$ n = 6 mice). **e**, Although neurons may have similar number of spikes during a certain time period of recording, the difference of their coefficient of variation unveils different firing patterns ranging from regular firing (Cell 1) to bursty firing (Cell 2). **f**, The coefficient of variation of IEI (by calcium imaging) highly correlates with the coefficient of variation of ISI (by Ephys) (n = 36 cells; $R^2 = 0.38$, $P = 0.0001$, $\rho = 0.61$, Pearson's correlation coefficient). **g**, Cumulative distribution of IEI (the first 5s, zoom-in from **d**) of the top 10% highly active neurons and the remaining 90% neurons (in Ctx A) at 5h or 2d after the context A exposure. The difference between the top 10% most active and the remaining 90% neurons in Ctx A was strongly reduced from 5h to 2d in WT mice but not in *Ccr5*$^{-/-}$ mice (WT n = 5, *Ccr5*$^{-/-}$ n = 6 mice). **h**, Coefficient of variation from the top 10% most active neurons (normalized to the remaining 90%). WT or *Ccr5*$^{-/-}$ mice were exposed to Ctx B 5h or 2d after Ctx A. WT mice showed a significant decrease in the coefficient of variation of IEI comparing the data for the 2d and 5h intervals, whereas *Ccr5*$^{-/-}$ mice had similar coefficient of variation of IEI in both intervals (WT n = 5, *Ccr5*$^{-/-}$ n = 6 mice; *$P < 0.05$, two-way repeated measures ANOVA). All results shown as mean ± s.e.m.

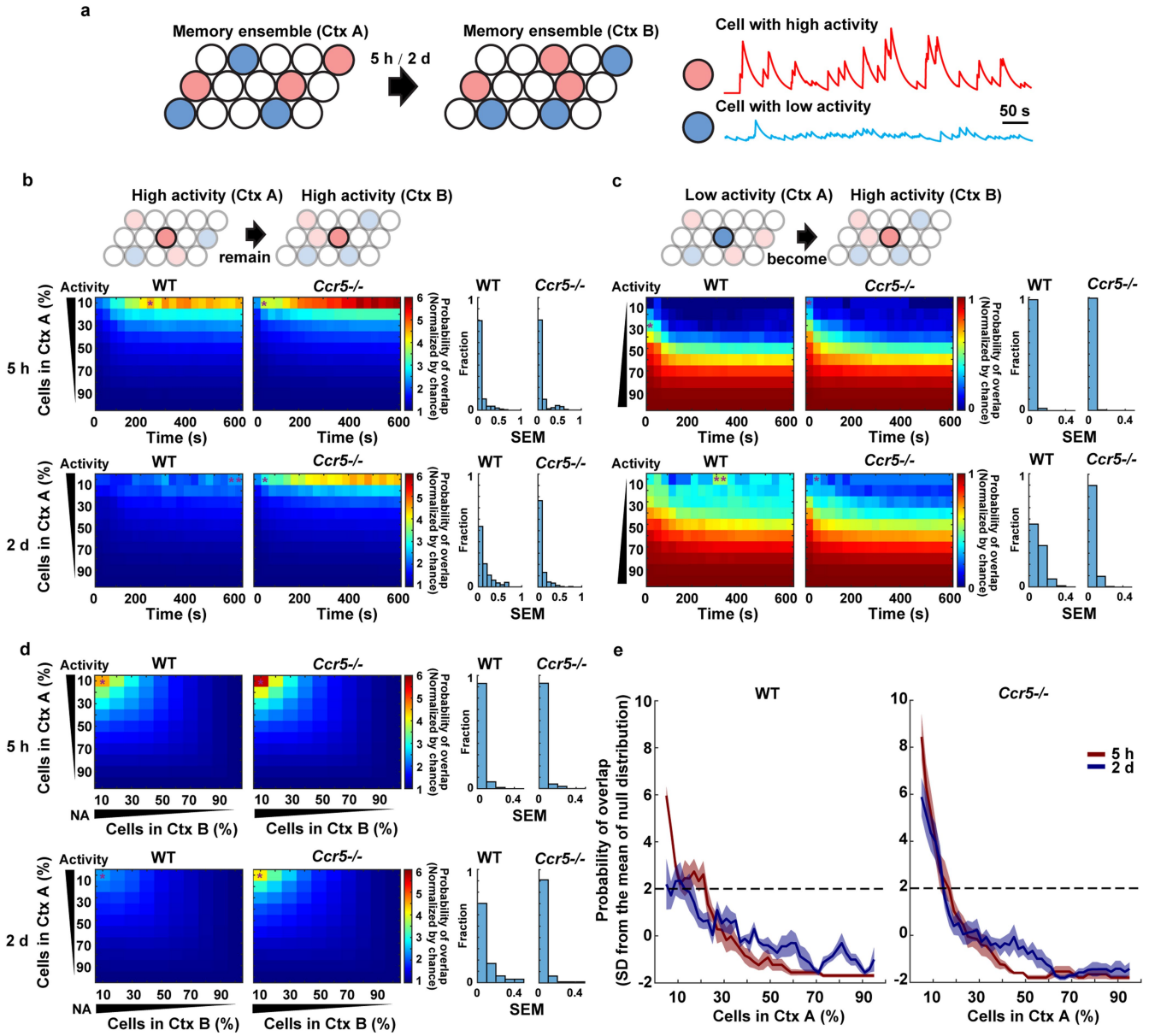

Extended Data Fig. 9 | Analysis of neuronal activity and overlap probability in wild-type and *Ccr5* knockout mice. a, Schematics showing that cells in neuronal ensembles can be sorted into cells with high neuronal activity (red) and low activity (blue), based on their average activity during the exploration of Ctx A and Ctx B which were separated by either a 5h or 2d interval. **b**, **c**, Left: Probability of overlap (averaged across mice) between subsets of cells with different levels of activity (y axis) during exploration of Ctx A and Ctx B, in WT and *Ccr5*$^{-/-}$ mice across time in Ctx B (x axis). Colour bars refer to normalized probabilities (chance = 1). Cumulative values were used for x and y axis (e.g., for x axis, 200s means 0–200 s; for y axis, 30 refers to the neurons within the top 30% of high (**b**) or low (**c**) activity). Right: the distribution of SEM across mice for the figures on the left. Asterisks (in the probability of overlap figures) represent the maximum SEM from each plot (WT n = 5, *Ccr5*$^{-/-}$ n = 6 mice). **b**, Probability of overlap between high activity cells in Ctx A and high activity cells in Ctx B in WT and *Ccr5*$^{-/-}$ mice. Note that the top 10% high activity cells in Ctx A are very likely to remain within the top 10% high activity cells in Ctx B 5h later for both WT and *Ccr5*$^{-/-}$ mice. In contrast, this subset of cells was reactivated around chance levels 2d later in Ctx B in WT mice, but not in *Ccr5*$^{-/-}$ mice. In the *Ccr5*$^{-/-}$ mice this subset of cells was still very likely to remain within the top 10% high activity cells in Ctx B. **c**, Probability of overlap between low activity cells in Ctx A and high activity cells in Ctx B in WT and *Ccr5*$^{-/-}$ mice. In contrast to high activity cells in Ctx A, the low activity cells in Ctx A were less likely (compared to chance) to be within the high activity cells in Ctx B. **d**, The probability of overlap between different ensembles (Ctx A and Ctx B) was sorted by neuronal activity in Ctx A and Ctx B, with a 5h or 2d interval between the two contextual exposures. Cells were sorted in percentages from top to bottom mean neuronal activity in the first context (Ctx A, y axis) and from left to right in the second context (Ctx B, x axis). With a 5h interval between Ctx A and B, the likelihood that neurons with high activity in Ctx A remained with high activity in Ctx B was higher than chance for both WT and *Ccr5* knockout mice. With a 2d interval, the likelihood that neurons with high activity in Ctx A remained high activity in Ctx B was at chance levels in WT mice. In contrast, *Ccr5* knockout mice showed a pattern similar to that observed with the 5 h interval (WT n = 5, *Ccr5*$^{-/-}$ n = 6 mice). **e**, Cells were again sorted from high to low activity in Ctx A with a 10% sliding window and 2% steps. The probability of overlap between subsets of cells (10% ensemble size) from Ctx A and the ensemble cells with top 10% high activity in Ctx B was plotted. The probability values were z-scored with respect to a null distribution created by randomly subsampling 10% of cells from Ctx A 10,000 times (i.e., results are represented as standard deviation (SD) from the mean of the null distribution). The 2SD threshold is labelled with a dashed line (WT n = 5, *Ccr5*$^{-/-}$ n = 6 mice).

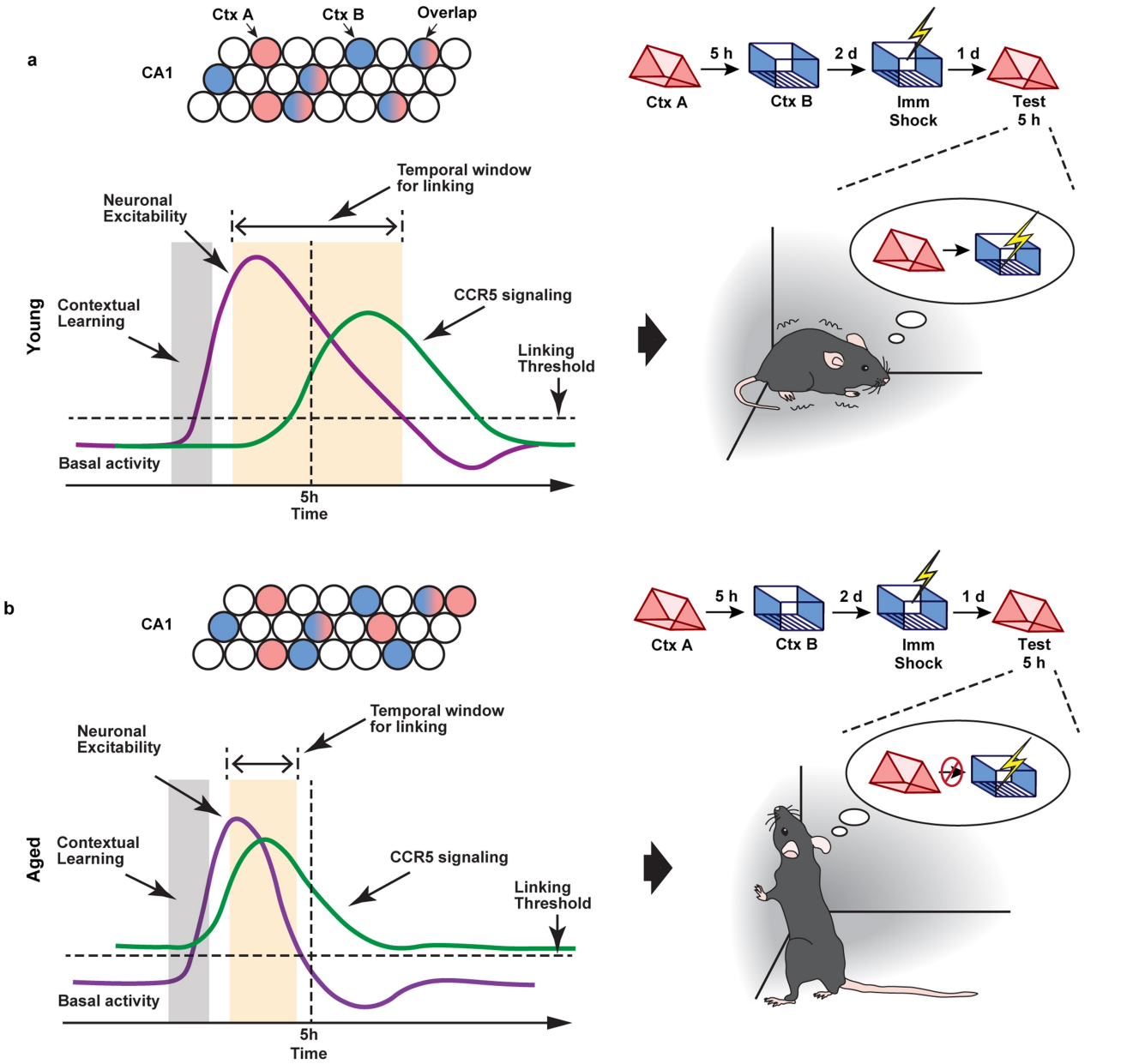

Extended Data Fig. 10 | Graphical abstract. a, In young mice, CCR5 signalling increases at a time point more than 5h after learning, and neuronal excitability and memory ensemble overlap remain high at 5h after learning. As a result, memories for context A (neutral context) and context B (shocked context) are linked together, and mice show high freezing during the test in context A. **b**, In aged mice, CCR5 signalling is higher than young mice at baseline and there is a further increase before 5h after learning, which lead to a reduction of neuronal excitability and memory ensemble overlap at 5h after learning. As a result, memories for context A (neutral context) and context B (shocked context) are not linked, and mice show low freezing during the test in context A.

nature portfolio

Corresponding author(s): Alcino Silva
Miou Zhou

Last updated by author(s): Mar 3, 2022

Reporting Summary

Nature Portfolio wishes to improve the reproducibility of the work that we publish. This form provides structure for consistency and transparency in reporting. For further information on Nature Portfolio policies, see our Editorial Policies and the Editorial Policy Checklist.

Statistics

For all statistical analyses, confirm that the following items are present in the figure legend, table legend, main text, or Methods section.

n/a	Confirmed
☐	☒ The exact sample size (*n*) for each experimental group/condition, given as a discrete number and unit of measurement
☐	☒ A statement on whether measurements were taken from distinct samples or whether the same sample was measured repeatedly
☐	☒ The statistical test(s) used AND whether they are one- or two-sided *Only common tests should be described solely by name; describe more complex techniques in the Methods section.*
☒	☐ A description of all covariates tested
☐	☒ A description of any assumptions or corrections, such as tests of normality and adjustment for multiple comparisons
☐	☒ A full description of the statistical parameters including central tendency (e.g. means) or other basic estimates (e.g. regression coefficient) AND variation (e.g. standard deviation) or associated estimates of uncertainty (e.g. confidence intervals)
☐	☒ For null hypothesis testing, the test statistic (e.g. *F*, *t*, *r*) with confidence intervals, effect sizes, degrees of freedom and *P* value noted *Give P values as exact values whenever suitable.*
☒	☐ For Bayesian analysis, information on the choice of priors and Markov chain Monte Carlo settings
☒	☐ For hierarchical and complex designs, identification of the appropriate level for tests and full reporting of outcomes
☐	☒ Estimates of effect sizes (e.g. Cohen's *d*, Pearson's *r*), indicating how they were calculated

Our web collection on statistics for biologists contains articles on many of the points above.

Software and code

Policy information about availability of computer code

Data collection	NIS-Elements AR (Nikon,v4.40.00), DAQ software (written in C++ andOpen Computer Vision libraries for mini-scope image acquisition, v0.171), Video Fear Conditioning "Video Freeze®" Software (Med Associates), ephys: pCLAMP 10 and Digidata® 1440A
Data analysis	Nikon NIS-Elements AR Analysis (v4.40.00), ImageJ (v1.53f51), Matlab R2020b (v9.9.0.1524771), ephys: Stimfit (v0.15.8), Graphpad Prism6, Almeida-FilhoDG/ConcatMiniscope (v1.0.0, DOI: 10.5281/zenodo.5676164)

For manuscripts utilizing custom algorithms or software that are central to the research but not yet described in published literature, software must be made available to editors and reviewers. We strongly encourage code deposition in a community repository (e.g. GitHub). See the Nature Portfolio guidelines for submitting code & software for further information.

Data

Policy information about availability of data

All manuscripts must include a data availability statement. This statement should provide the following information, where applicable:

- Accession codes, unique identifiers, or web links for publicly available datasets
- A description of any restrictions on data availability
- For clinical datasets or third party data, please ensure that the statement adheres to our policy

The original videos and datasets generated during and/or analyzed during the current study are available from the corresponding authors.
We choose to share data on request due to the fact that video recording files are very large and hard to access online. Additionally, our data includes complex and diverse experimental conditions, and our lab can best help people access the data according to their specific requests.

Field-specific reporting

Please select the one below that is the best fit for your research. If you are not sure, read the appropriate sections before making your selection.

☒ Life sciences ☐ Behavioural & social sciences ☐ Ecological, evolutionary & environmental sciences

For a reference copy of the document with all sections, see nature.com/documents/nr-reporting-summary-flat.pdf

Life sciences study design

All studies must disclose on these points even when the disclosure is negative.

Sample size	No sample size precalculation was performed. Sample sizes were chosen as standard in the field. These numbers were derived with literature searches for similar experiments and also from our extensive experience with the techniques and approaches used, including molecular/biochemical analysis, electrophysiology, in vivo imaging with head mounted fluorescent miniscopes and behavioral analyses. Briefly, 6-18 mice per group for behavior test. For biochemical experiments, at least 3 mice were used for each group. In several cases (especially control mice), number of animals exceeded this standard since several batches of mice were tested independently and pooled together for final analysis.
Data exclusions	Data were excluded out based on outliers test (Grubbs' test, 95% confidence) supplied by GraphPad. For behavior task, mice with high freezing (>20% of 10 min) during pre-exposure (without shock) were excluded due to abnormally high level of anxiety.
Replication	Experiments were repeated, and the results are reproducible. Briefly, for behavior task, each result was collected from at least 2 independent experiments. Representative histological images were repeated independently in different mice (no less than 3) with similar results. Representative in vitro experiments were biologically duplicated.
Randomization	Across experiments, mice were randomly assigned to experimental vs. control groups in behavioral training, anatomical, optogenetic and miniscope studies with matched age and sex, whenever possible. For in vitro experiments, cultured cell dishes were also randomly assigned to control and different experimental groups.
Blinding	During the experiment and analysis, all experiments were performed blindly.

Reporting for specific materials, systems and methods

We require information from authors about some types of materials, experimental systems and methods used in many studies. Here, indicate whether each material, system or method listed is relevant to your study. If you are not sure if a list item applies to your research, read the appropriate section before selecting a response.

Materials & experimental systems

n/a	Involved in the study
☐	☒ Antibodies
☐	☒ Eukaryotic cell lines
☒	☐ Palaeontology and archaeology
☐	☒ Animals and other organisms
☒	☐ Human research participants
☒	☐ Clinical data
☒	☐ Dual use research of concern

Methods

n/a	Involved in the study
☒	☐ ChIP-seq
☒	☐ Flow cytometry
☒	☐ MRI-based neuroimaging

Antibodies

Antibodies used	chicken polyclonal anti-GFP (Abcam AB13970, 1:1000), mouse anti-Neun NeuN (Chemicon,MAB377, 1:1000), rabbit anti-GFAP (Dako, Z0334 1:500), rabbit anti-P2Y12 (AnaSpec, AS-55043A, 1:1000),rabbit anti-c-Fos (Cell signaling, 9F6, #2250, 1:500), rabbit anti-pErk (Cell signaling, #9101, 1:2000), rabbit anti-Erk (Cell signaling, #9102, 1:2000), mouse anti-β-actin (Sigma-Aldrich, A5316, 1:10,000), chicken anti-RFP (Synaptic Systems, 409 006, 1:500), mouse anti-TetR Monoclonal Antibody (Clone 9G9, Takara, 631131, 1:500), goat anti-chicken 488 (Invitrogen, A11039, 1:2000), goat anti-mouse 488 (Invitrogen, A11029, 1:2000), goat anti-chicken 594 (Invitrogen, A11042, 1:2000), goat anti-rabbit 647 (Invitrogen, A21245, 1:2000), goat anti-mouse HRP (Bio Rad, 170-6516, 1:10000) and goat anti-rabbit HRP (Bio Rad, 170-6515, 1:5000)
Validation	Chicken polyclonal anti-GFP, mouse anti-Neun NeuN and rabbit anti-GFAP has been used in our previous publication (Miou Zhou, er al. elife, 2016) Rabbit anti-P2Y12 has been used in other publication (e.g., Jiyun Peng, et al. Molecular Brain,2019) Rabbit anti-c-Fos has been widely used in many publications (e.g., Denise J. Cai, et al. nature, 2013; Laura E Mickelsen, et. al. Nat Neurosci, 2019)

Rabbit anti-pErk, Rabbit anti-Erk and Mouse anti-β-actin has been used in our previous publication (Yong-Seok Lee, et al. Nat Neurosci, 2014)
Chicken anti-RFP has been used in other publication (e.g. Bakr M, et al. Cell reports,2021)
Mouse anti-TetR Monoclonal Antibody has been used in other publication (e.g., Sander B Frank, et al. BMC Biotechnol ,2017)

Eukaryotic cell lines

Policy information about cell lines

Cell line source(s)	HEK293 is kindly provided by Dr. Corinna Burger at University of Wisconsin-Madison
Authentication	None of the cell lines used were authenticated
Mycoplasma contamination	None of the cell lines used were not tested for mycoplasma contamination
Commonly misidentified lines (See ICLAC register)	None of the cell lines used were not tested for mycoplasma contamination

Animals and other organisms

Policy information about studies involving animals; ARRIVE guidelines recommended for reporting animal research

Laboratory animals	Mus musculus (1) C57BL/6NTac (both male and female, age 11-16 weeks), (2) C57BL/6NIA (male, age16-18 months), (3) B6.129P2-Ccr5tm1Kuz N10 from Taconic Farms (both male and female, age 11-16 weeks and age16-18 months), (4) cFos-tTa mice in a C57BL/6N background (both male and female, age 3-6 months), (5) B6.129P2-Ccl5tm1Hso/J from Jackson lab (both male and female, age ~2-3 months) Mice are housed in AAALAC accredited facility with 12-12 light/dark cycles. Housing conforms to The Guide for the Care and Use of Laboratory Animals, 8th edition. The temperature setpoint is 72 degrees plus or minus 3 degrees; the humidity range is between 30% to 70%.
Wild animals	No Wild animals were used
Field-collected samples	No field-collected samples were used in this study
Ethics oversight	All experimental protocols were approved by the Chancellor's Animal Research Committee of the University of California, Los Angeles, in accordance with NIH guidelines.

Note that full information on the approval of the study protocol must also be provided in the manuscript.